CrystEngComm

Cite this: *CrystEngComm*, 2012, **14**, 8468–8484

www.rsc.org/crystengcomm

PAPER

Comprehensive studies of non-covalent interactions within four new Cu(II) supramolecules†

M. Mirzaei,*[a] H. Eshtiagh-Hosseini,[a] M. Chahkandi,*[b] N. Alfi,[a] A. Shokrollahi,[c] N. Shokrollahi[c] and A. Janiak[d]

Received 5th September 2012, Accepted 17th September 2012
DOI: 10.1039/c2ce26442k

This work investigates the supramolecular aggregation of Cu(II) complexes based on a combination of the heterocyclic N-donor ligand 2-aminopyrimidine (2-apym) and a variety of different carboxylate ligands, like salicylic acid (H_2SAL), maleic acid (H_2MAL), and glycine (HGLY). Four new Cu(II) complexes $[Cu(HSAL)_2(2\text{-apym})_2]$ (**I**), $[Cu(HSAL)_2(2\text{-apym})_2]\cdot(H_2SAL)_2(2\text{-apym})$ (**I′**), $\{(H2\text{-apym})[Cu(GLY)(\mu\text{-}Cl)_2Cl]\}_n$ (**II**) and $[Cu(\mu\text{-}MAL)(2\text{-apym})]_n$ (**III**) have been synthesized and characterized by elemental analyses, FT-IR spectra, and X-ray structural analyses. **I** and **I′** appear as molecular clusters whereas **II** is a 1-D coordination polymer with weak axial Cu–Cl interactions. However the last one shows a 2-D coordination polymer with trigonal bipyramidal geometry for Cu(II) ion. The two last cases have no molecular fragments packed with non-covalent interactions. In these new supramolecular compounds, existent species join together with the cooperation of multiple inter/intra-molecular classical O–H···O/N, N–H···O/N, and non-classical N–H···Cl hydrogen bonds (H-bonds), offset face to face π···π, edge to face C/N–H···π, and lp···π stacking interactions in the form of various homo/hetero-synthons leading to architecturally different structures. DFT calculations were used to estimate the binding energy of the involved non-covalent interactions and whole stabilization energy of related network of **I**, **I′**, and **II**. Theoretical calculations facilitate the comparison of intermolecular interactions, which demonstrate that for all of **I**–**II**, N–H···N and N–H···O H-bonds govern the network formation. The equilibrium constants for the three proton-transfer systems including SAL/2-apym, GLY/2-apym, MAL/2-apym, the stoichiometry and stability of complexation of these systems with Cu^{2+} ion in aqueous solution were investigated by potentiometric pH titration method. The stoichiometries of the most complex species in solution was compared to the crystalline Cu^{2+} ion complexes with the cited proton-transfer systems.

Introduction

In modern chemistry non-covalent interactions are determining in the field of supramolecular chemistry and molecular recognition. Non-covalent interactions led to the formation of molecular clusters while covalent interactions led to classical molecules. Formation of a non-covalent cluster does affect properties of the subsystems, and these changes are important for the detection of cluster formation. Non-covalent interactions were firstly recognized by van der Waals in the 19th century[1] and helped to reformulate the equation of state for real gases. Hydrogen bonds (H-bonds), π···π stacking, cation···π, and a new type of van der Waals interactions namely the anion···π (for short lp···π) as non-covalent interactions form the backbone of supramolecular chemistry. H-bonds that play a central role in the structure, function, and dynamics of chemical and biological systems,[2] cation···π interactions which are supposed to be decisive in the ion selectivity of potassium channels,[3] anion···π interactions that support the theoretical prediction and promising proposal for use of anion receptors in molecular recognition[4] and π···π interactions presence in the folding of proteins[5] in the structure of DNA as well as in its interaction with small molecules, are used in crystal engineering for the design of functional materials.[6] Molecular functionalities, *e.g.* amino, hydroxyl, carboxylate, play essential roles in studying the spatial relationship between adjacent fragments resulting in repetitive van der Waals patterns or supramolecular synthons.[2] Many of the synthons in crystal networks of metal–organic compounds contain classical and non-classical H-bonds as well as stacking,

[a]*Department of Chemistry, Ferdowsi University of Mashhad, 917791436, Mashhad, Iran. E-mail: mirzaeesh@um.ac.ir*
[b]*Department of Chemistry, Hakim Sabzevari University, Sabzevar, 96179-76487, Iran. E-mail: chahkandimohammad@gmail.com*
[c]*Department of Chemistry, Yasouj University, Yasouj, Iran*
[d]*Department of Chemistry, Adam Mickiewicz University, Grunwaldzka 6, Poznań, 64-510, Poland*

† Electronic supplementary information (ESI) available: Pertinent figures of frameworks formation of **I**, **I′**, **II**, and **III** compounds *via* different H-bonding and stacking interactions together with stabilization and formation calculated energies. CCDC 893822, 893823, 827999, and 893821. For ESI and crystallographic data in CIF or other electronic format see DOI: 10.1039/c2ce26442k

Table 1 Crystal data and data collection, refinement parameters for the complexes

	I	I′	II	III
Empirical formula	$C_{22}H_{20}CuN_6O_6$	$C_{58}H_{54}CuN_{12}O_{18}$	$C_6H_{10}Cl_2CuN_4O_2$	$C_8H_7Cu_1N_3O_4$
FW	527.98	1270.67	304.62	272.70
Temp/K	294.0(1)	295.5(1)	120(2)	150 (2)
λ/Å	0.71073	0.71073	0.71073	1.54184
Cryst. syst.	Monoclinic	Triclinic	Orthorhombic	Monoclinic
Space group	$P2_1/n$	$P\bar{1}$	$Pbca$	$P2_1/c$
Cryst. size/mm^3	0.38 × 0.30 × 0.07	0.55 × 0.30 × 0.20	0.40 × 0.20 × 0.20	0.22 × 0.20 × 0.14
a/Å	9.9258(2)	7.6075(2)	12.4940(6)	10.0366 (7)
b/Å	12.0698(3)	9.9472(4)	7.5099(4)	9.1255 (7)
c/Å	20.1039(6)	20.8858(8)	22.6355(11)	10.2985 (7)
α/°	90.00	81.235(3)	90.00	90.00
β/°	97.815(3)	82.268(3)	90.00	95.832 (5)
γ/°	90.00	72.818(3)	90.00	90.00
V/Å^3	2386.13(10)	1485.61(9)	2123.86(18)	938.35 (12)
Z	4	1	8	4
d_{calcd}/mg m^{-3}	1.470	1.420	1.905	1.930
Abs coeff/mm^{-1}	0.97	0.45	2.54	3.32
θ/°	2.96, 28.91	2.97, 30.71	3.15, 27.53	6.57, 66.64
h	$-11 \leqslant h \leqslant 13$	$-10 \leqslant h \leqslant 10$	$-8 \leqslant h \leqslant 14$	$-9 \leqslant h \leqslant 19$
k	$-16 \leqslant k \leqslant 16$	$-14 \leqslant k \leqslant 14$	$-8 \leqslant k \leqslant 4$	$-10 \leqslant k \leqslant 10$
l	$-26 \leqslant l \leqslant 17$	$-29 \leqslant l \leqslant 29$	$-26 \leqslant l \leqslant 21$	$-11 \leqslant l \leqslant 12$
R_{int}	0.0412	0.0216	0.0356	0.0386
GOF	1.03	1.05	0.85	1.07
Final R_1, wR_2 [$I > 2\sigma$ (I)]	0.0508, 0.0960	0.0374, 0.00991	0.0302, 0.0601	0.031, 0.083

Table 2 Selected experimental and calculated atomic distances (Å) and angles (°) for **I–III**

	Experimental	Calculated		Experimental	Calculated
I					
Cu1–O1	1.779(3)	1.730	O3–C3	1.349(4)	1.354
Cu1–O2	1.780(3)	1.741	O13–C13	1.354(3)	1.286
Cu1–O11	2.392(3)	2.282	O11–Cu1–O1	177.38(8)	178.20
Cu1–O12	2.384(3)	2.275	O11–Cu1–N21	87.80(9)	88.13
Cu1–N21	2.325(3)	2.339	O1–Cu1–N21	90.64(9)	90.37
Cu1–N31	2.359(3)	2.291	O11–Cu1–N31	91.52(9)	90.65
O1–C1	2.546(3)	2.479	O1–Cu1–N31	90.12(9)	91.24
O11–C11	1.276(6)	1.252	O2–Cu1–N21	177.61(9)	176.70
O12–C11	1.292(6)	1.237			
I′					
Cu1–O1	1.9887(9)	1.889	O1–Cu1–O1	180.0	179.31
Cu1–O2	1.780(3)	1.691	O1–Cu1–N11	87.14(4)	89.54
Cu1–N11	2.0104(11)	1.910	O1–Cu1–N11	92.86(4)	91.03
O1–C1	1.2610(15)	1.198	N11–Cu1–N11	180.00(3)	178.4
II					
Cu1–N1	1.980(4)	1.881	N1–Cu1–O1	83.12(13)	85.71
Cu1–O1	1.982(2)	1.883	N1–Cu1–Cl2	91.21(1)	90.24
Cu1–Cl2	2.255(11)	2.164	N1–Cu1–Cl1	169.28(11)	169.80
Cu1–Cl1	2.2725(11)	2.174	O1–Cu1–Cl2	166.49(8)	165.3
O1–C1	1.269(4)	1.235	O1–Cu1–Cl1	88.25(7)	87.81
O2–C1	1.249(4)	1.196			
III					
Cu1–O4	1.9388(16)	—	O4–Cu1–O3^{i}	176.23(7)	—
Cu1–O3^{i}	1.9512(16)	—	O4–Cu1–O2^{ii}	96.07(7)	—
Cu1–O2^{ii}	1.9728(18)	—	O3^{i}–Cu1–O2^{ii}	87.60(7)	—
Cu1–O1^{i}	2.0562(16)	—	O4–Cu1–O1^{i}	90.31(7)	—
Cu1–N11	2.1462(19)	—	O3^{i}–Cu1–O1^{i}	87.76(7)	—
O1–C1	1.260(3)	—	O2^{ii}–Cu1–O1^{i}	133.27(7)	—
O2–C1	1.250(3)	—	O4–Cu1–N11	90.34(7)	—
O3–C3	1.256(3)	—	O3^{i}–Cu1–N11	86.76(7)	—
O4–C3	1.264(3)	—	O2^{ii}–Cu1–N11	127.17(7)	—
O1^{i}–Cu1–N11	98.92(7)	—			

Symmetry codes: (i) $-x$, $y - 1/2$, $-z + 1/2$; (ii) $-x$, $-y + 1$, $-z$.

which provide the requisite robustness and reproducibility to create novel solid-state structures. In this work, glycine, maleic, and salicylic acids have been used for synthesizing new complexes because they can hold together interactive functional groups for the formation of a variety of one-dimensional (1-D), two-dimensional (2-D), and three-dimensional (3-D) architectures based on multiple non-covalent interactions. Indeed, these sophisticated spatial directions within related complexes resulting in different contacts with neighboring molecules would be useful tools in new structure designing within crystal engineering concepts. Modern *ab initio* quantum chemistry has been very successful in describing the electronic structure of isolated molecules in agreement with experimental results. The stronger non-covalent interaction causes larger changes in the properties of the subsystem. The majority of molecular clusters are non-rigid systems, and hence, the potential energy surface represents their primary property. Structures of global and local minima of the surface are found by optimizing the stabilization energy and not the total energy. Therefore, stabilization energy plays central role in non-covalent interactions.[7] Successes and failures of DFT (density functional theory) in studies of H-bonded and stacked structures have been demonstrated on DNA base pairs and amino acid pairs. DFT calculations are much faster than correlated WFT (wave function theory) calculations and do not depend so heavily on the basis set size; furthermore, additional speedups can be gained by using GGA functional (like BLYP, BP86, *etc.*) A very promising approach entails a combination of DFT-D (dispersion energy corrected). This procedure is fast and can even be used in on-the-fly *ab initio* (DFT-D) molecular dynamics simulations. This technique is a very promising tool for studies of the dynamic properties of small and medium non-covalent complexes.[8] In recent years, the design of systematic pathways to obtain supramolecular networks such as metal–organic frameworks (MOFs), coordination polymers (CPs), and other geometries due to their diverse potential applications, unprecedented architectures, and various topologies are great of attention and rapidly growing the novel research area.[9–17] From crystal engineering view point, O-, N-, and S-donor organic multifunctional ligands are the best candidates for possible infinite expansion of supramolecular architectures having different dimensionality.[18–21] Over the past decade, our research group has been interested in the syntheses, structural features, and crystal engineering of the coordination compounds obtained *via* proton-transfer mechanism between organic ligands.[22] Rational selection of appropriate acidic and basic ligands having ΔpK_a (pK_a (D–H) − pK_a (A–H$^+$)) greater than 2 or 3 has obvious significance. In general, versatile functional organic ligands can establish strong coordination ability, H-bonding, and stacking which are driving forces for supramolecular networks.[23–26] Theoretical calculations can respond to the request to determine the optimized structure of the cluster, its stabilization energy, its (intermolecular) vibrational frequencies and the potential and free energy surfaces.[27] For understanding the role of the latter contacts with diverse distance ranges and directionalities on crystal network formation, using ligands of salicylic acid, maleic acid, glycine, and heterocyclic N-donor 2-aminopyrimidine high level theoretical calculations were carried out for better clarification of the

Table 3 H-bond parameters (Å, °)

D–H···A	*d*(D–H)	*d*(H···A)	*d*(D···A)	<(DHA)
I				
O3–H3···O1	0.99	1.61	2.546(3)	157
O13–H13···O12	1.00	1.65	2.572(3)	151
N22–H22A···N33[1]	0.86	2.24	3.086(3)	170
N22–H22B···O2	0.97	2.32	3.185(3)	148
N32–H32A···N23[2]	0.90	2.09	2.989(3)	176
N32–H32B···O13[3]	0.93	2.28	3.106(3)	147
N32–H32B···O12	0.93	2.46	3.208(3)	137
I′				
O3–H3···O2	0.90	1.68	2.5269(14)	156
N12–H12A···N13[4]	0.88	2.13	3.0161(16)	179
N12–H12B···O3[5]	0.81	2.28	3.0062(17)	149
O22–H22···N43[6]	0.88	1.79	2.658(2)	175
O23–H23···O21	0.97	1.70	2.584(2)	151
O32–H32···N41[7]	0.89	1.76	2.638(2)	171
O33–H33···O31	0.90	1.73	2.586(2)	157
N42–H42A···O21[8]	0.87	2.10	2.950(2)	166
N42–H42B···O31[7]	0.88	2.15	3.012(2)	166
II				
N1–H1N1···Cl1[9]	0.91(5)	2.35(5)	3.244(4)	167(4)
N1–H1N2···Cl1[10]	0.77(4)	2.66(4)	3.335(4)	147(4)
N4–H4N1···N2[11]	0.82(4)	2.18(4)	2.988(5)	172(5)
N4–H4N2···O1	0.77(5)	2.12(4)	2.873(4)	169(5)
N3–H3N···O2	0.77 (4)	1.89(5)	2.645(4)	166(5)
III				
N12–H122···N13[12]	0.853	2.24(3)	3.077(4)	171(3)

Symmetry codes: (1) $x + 1, y, z$; (2) $x - 1, y, z$; (3) $-x + 1, -y, -z + 1$; (4) $-x + 1, -y + 1, -z + 1$; (5) $x + 1, y, z$; (6) $x + 1, y - 1, z$; (7) $-x, -y + 1, -z$; (8) $x - 1, y + 1, z$; (9) $-x + 1/2, y - 1/2, z$; (10) $x + 1/2, y, -z + 1/2$; (11) $-x, -y + 1, -z + 1(3)$; (12) $-x + 1, -y, -z$.

Table 4 The non-covalent interactions distances (Å), angles (°), and binding energies (kcal mol^{-1}) calculated with B3LYP-D/triple-ζ6-311+G(d,p)

	d(H···A)	<(DHA)	Binding energy
I			
N_{32}–H_{32}···N_{23}	1.880	175.67	−59.73
N_{22}–H_{22}···N_{33}	2.019	174.36	−55.60
C_{25}–H_{25}···π	2.299	152.64	−46.98
C_6–H_6···π	3.092	135.43	−36.42
I′			
O_{32}–H_{32}···N_{41}	1.582	171.03	−71.28
O_{32}–H_{32}···N_{42}	1.599	178.19	−70.21
O_{22}–H_{22}···N_{43}	1.607	173.89	−69.87
N_{42}–H_{42A}···O_{21}	1.887	166.84	−59.51
N_{12}–H_{12A}···N_{13}	1.919	177.66	−58.50
N_{42}–H_{42B}···O_{31}	1.933	166.38	−56.73
C_{35}–H_{35}···π	3.047	126.17	−37.08
N_{42}–H_{42A}···π	3.053	97.02	−36.78
C_{36}–H_{36}···π	3.093	170.54	−36.30
C_{34}–H_{34}···π	3.151	154.02	−35.69
C_{44}–H_{44}···π	3.166	142.51	−35.46
C_6–H_6···π	3.239	137.72	−34.67
C_{45}–H_{45}···π	3.325	138.58	−33.78
N_{42}–H_{42B}···π	3.430	75.62	−31.80
II			
N_4–H_4···O_1	1.581	177.03	−78.98
N_3–H_3···O_2	1.801	168.18	−74.82
N_4–H_4···N_2	1.773	167.29	−63.37
N_4–H_4···Cl_1	2.396	145.25	−46.98
N_1–H_1···Cl_1	2.697	145.25	−41.63
π···π	3.452	180.00	-32.53

essential roles of used functional groups in the final stabilization gained by the titled crystal networks.

Experimental section

Materials and general methods

All reagents were purchased from Merck Chemicals and used without further purification. Infrared spectra were recorded on a Bomem B-154 Fourier transform spectrometer using KBr discs. Elemental analyses were performed with a Thermo Finnigan Flash-1112EA microanalyzer. A Model 794 Metrohm Basic Titrino was attached to an extension combined glass-calomel electrode mounted in an air-protected, sealed, thermostated jacketed cell maintained at 25.0 ± 0.1 °C by circulating water, from a constant-temperature bath Fisherbrand model FBH604, LAUDA, Germany, equipped with a stirrer and a 10.000 mL-capacity Metrohm piston burette. The pH meter-electrode system was calibrated to read $-\log [H^+]$.

Preparation

Preparation of complexes. $[Cu(HSAL)_2(2\text{-apym})_2]$ (I) and $[Cu(HSAL)_2(2\text{-apym})_2]\cdot(H_2SAL)_2(2\text{-apym})$ (I′). These two new complexes are obtained from solution containing H_2SAL (0.22 mmol, 0.03 g), 2-apym (0.42 mmol, 0.04 g) and aqueous solution of $CuCl_2\cdot 6H_2O$ (0.04 mmol, 0.01 g). After 24 h, by recrystallization of the first observed purple crystals, two types of appropriate purple plate-like (**I**) and dark-blue block-shape crystals (**I′**) was collected for X-ray studies (yield: 38.2% and 30.5% for **I** and **I′** respectively based on H_2SAL). Elem. Anal. Calc. for $C_{22}H_{20}CuN_6O_6$ (**I**): C, 50.00; H, 3.79; N, 15.90. Found: C, 50.12; H, 3.83; N, 16.15%. Elem. Anal. Calc. for $C_{58}H_{54}N_{12}O_{18}Cu$ (**I′**): C, 54.77; H, 4.25; N, 13.22. Found: C,

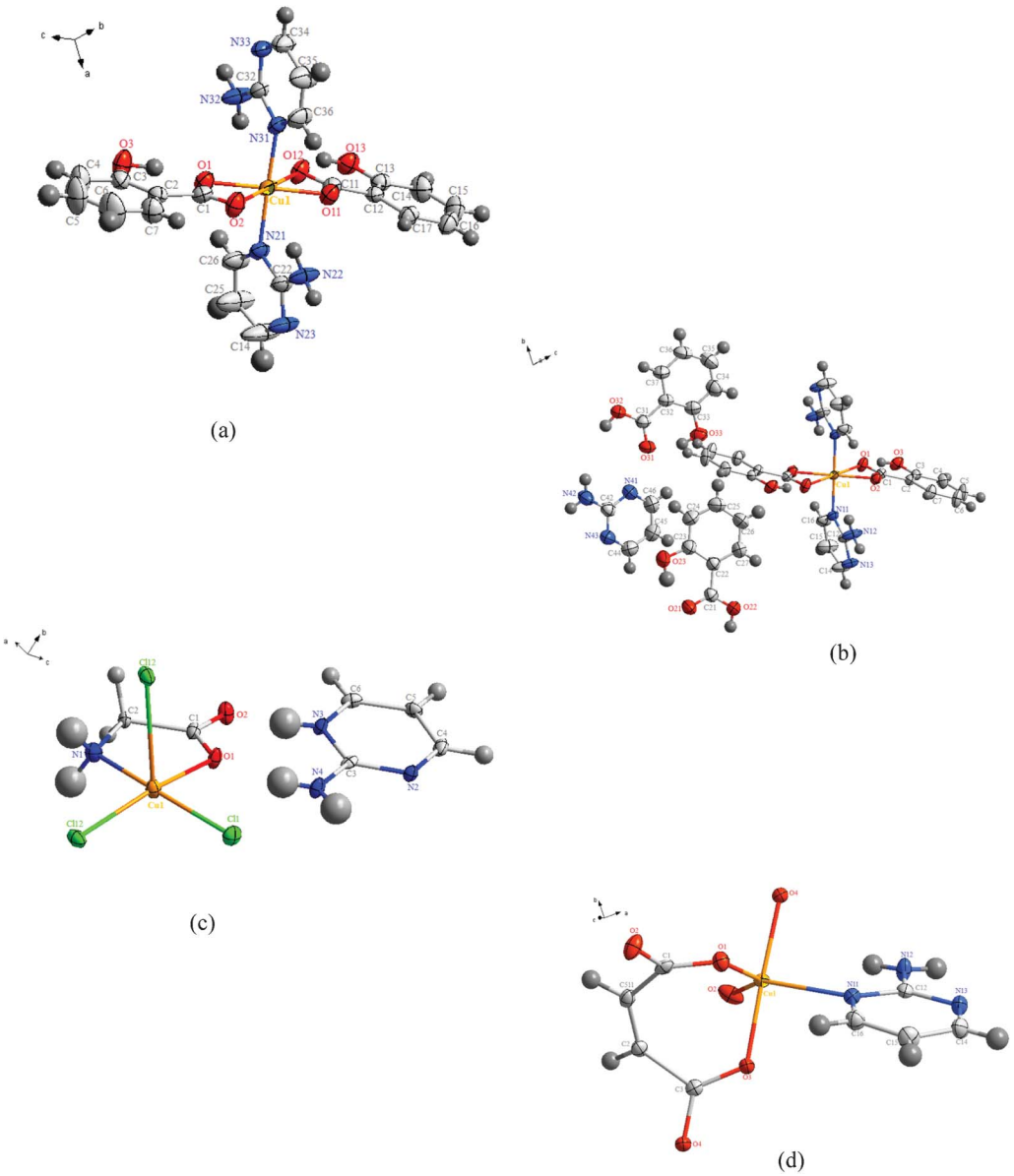

Fig. 1 Coordination environments of Cu(II) ions in **I** (a), **I′** (b), **II** (c), and **III** (d) with the atom numbering scheme for complexes (50% probability criterion for the thermal ellipsoids).

54.28; H, 4.37; N, 13.37%. IR (KBr pressed pellet, cm^{-1}, (**I**): 3400(s), 3300(w), 3200(w), 1665(w), 1645(w), 1610(w), 1570(s), 1480(s), 1465(w), 1400(w), 1365(w), 1340(s), 1255(w), 1170(w), 1150(s), 865(s), 820(s), 770(s), 425(w). IR (KBr pressed pellet, cm^{-1}, (**I′**): 3400(s), 3350(w), 3200(sh), 1660(sh), 1600(w), 1550(w), 1480(s), 1465(w), 1400(s), 1360(w), 1300(s), 1255(w), 1250(s), 1160(s), 860(s), 860(s), 820(s), 755(s), 530(s), 465(w).

{(H2-apym)[Cu(GLY)(μ-Cl)Cl]}$_n$ (II). Blue needle like crystals of **II** were obtained after slow evaporation of the solution containing HGLY (0.39 mmol, 0.03 g), 2-apym (0.39 mmol, 0.04 g), and $CuCl_2 \cdot 6H_2O$ (0.13 mmol, 0.03 g) which refluxed for 6 h at 333 K. The isolated crystals were subjected to X-ray studies (yield: 41.7% for **II** based on GLY). Elem. Anal. Calc. for $C_6H_{10}Cl_2N_4O_2Cu$: C, 23.64; H, 3.28; N, 22.4. Found: C, 24.09; H, 3.76; N, 22.2%. IR (KBr pressed pellet, cm^{-1}): 3130(br), 2800(br), 1680(w), 1480(w), 1410(w), 1355(s), 1120(s), 1060(m), 1035(w), 910(s), 705(w), 639(s), 520(w), 475(s).

[Cu(μ-MAL)(2-apym)]$_n$ (III). This compound was prepared in a similar manner as described for **II** by refluxing of H_2MAL (0.26 mmol, 0.03 g), 2-apym (0.52 mmol, 0.05 g), and $CuCl_2 \cdot 6H_2O$ (0.06 mmol, 0.015 g) (yield: 34.7% for **III** based on MAL). Elem. Anal. Calc. for $C_8H_7N_3O_4Cu$: C, 35.2; H, 2.58; N, 15.40; Found: C, 35.62; H, 2.57; N, 15.67%. IR data (cm^{-1}): 3370(w), 3190(w), 1650(m), 1605(w),1660(vs), 1332(s), 1260(w), 1100(w), 753(w).

X-ray crystallography

The single crystal X-ray diffraction data were collected with Xcalibur, Eos (**I** and **I′**), Xcalibur, Sapphire 2, large Be window (**II**), and Rigaku Rapid II (**III**) diffractometers. The structures were solved by direct methods and refined with a full-matrix least-squares technique based on F^2 with the SHELXL-97 crystallographic software package.[28] Carbon bound hydrogen atoms were positioned geometrically and refined as riding atoms with their U_{iso} set to 1.2 U_{eq} of their parent atoms. Nitrogen bound hydrogen atoms were located in a difference Fourier map and refined with fixed isotropic parameters of U_{iso} = 0.05 Å^2 for compounds **II** and **III** and the remaining compounds were located geometrically and refined as riding model. Details of crystallography data are given in Table 1. The selected bond distances and angles together with the H-bond geometry are listed in Tables 2 and 3, respectively.

Computational details

Periodic quantum calculations were executed in a Linux environment employing the Gaussian 09[29] software with experimentally observed crystal geometry as input. For full DFT geometry optimization calculations the hybrid functional B3LYP[30–32] was used with the LANL2DZ basis set for the copper atom and the triple-ζ6-311+G(d,p) basis set for all other atoms. We have considered high spin density for the Cu(II) atom

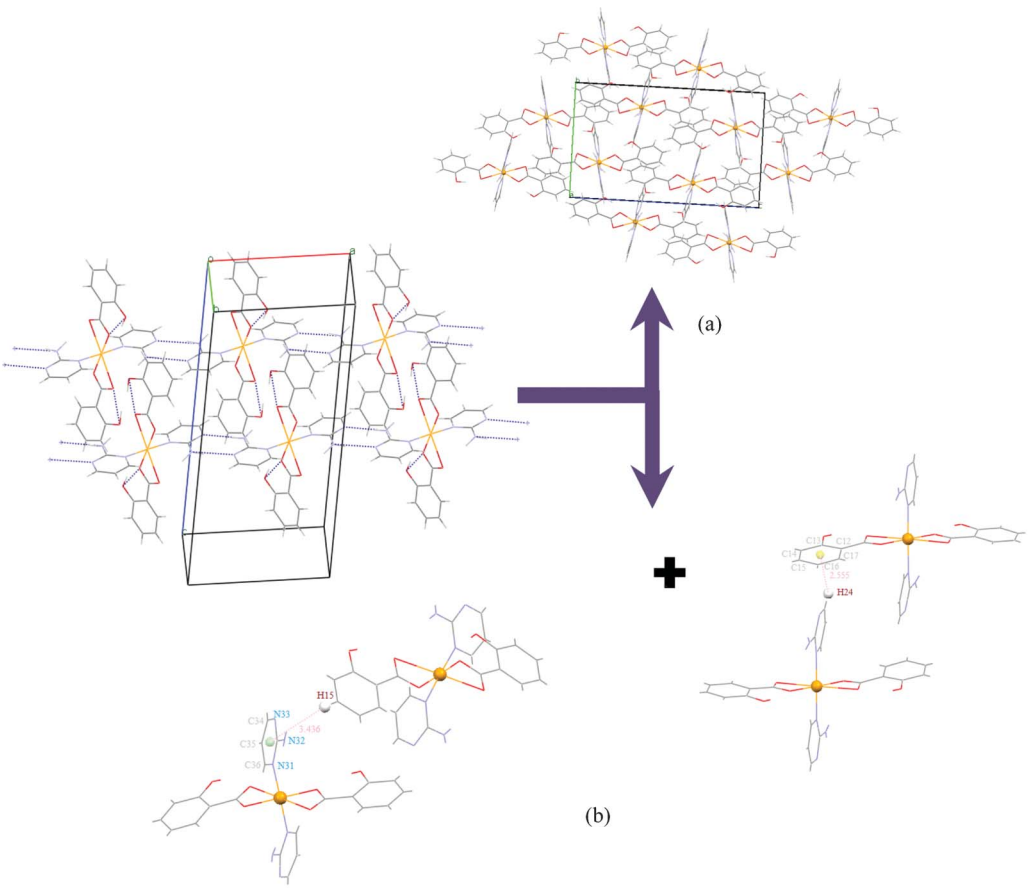

Fig. 2 A partial crystal packing diagram for **I** viewed parallel to the *ac* plane formed *via* H-bond interactions (H atoms have been omitted for clarity). (a) Illustration of the arrangement of complexes in **I**. (b) View of two kinds of C–H···π interactions.

for the calculations of all compounds. B3LYP method has been proved to provide accurate geometries and harmonic vibrational frequencies for a wide variety of hydrogen-bonded systems.[33] Binding energy calculations with correction for the basis set superposition error (BSSE) using the Boys–Bernardi counterpoise technique[34] were also performed using the B3LYP-D[35] functional as dispersion-corrected DFT. At first the structure of the smallest independent fragment of any complexes as monomer ($\mathbf{I}_{mon}$, $\mathbf{I'}_{mon}$, and $\mathbf{II}_{mon}$, Fig. 6–9) with the same molecular formula as the respective CIF has been optimized. In the following, for finding intermolecular interaction energies and geometry optimization, the smallest structures of network containing a number of corresponding monomers bearing all possible non-covalent interactions have been optimized. In Table 4 we summarize and compare the finding non-covalent interaction energies and related equilibrium distances and angles of any network.

Solution studies procedure

The details are described in ref. 36–39. The concentration of all ligands including SAL, GLY, MAL and 2-apym was 2.50×10^{-3} M for the potentiometric pH titrations of them in the absence and presence of 1.25×10^{-3} M Cu^{2+} ion in binary and ternary systems. A standard carbonate-free NaOH solution (0.09300 M) was used in all titrations. The ionic strength was adjusted to 0.1 M with $NaNO_3$. Before measuring of an experimental point (pH), sufficient time was allowed for the establishment of equilibrium. Protonation constants of ligands

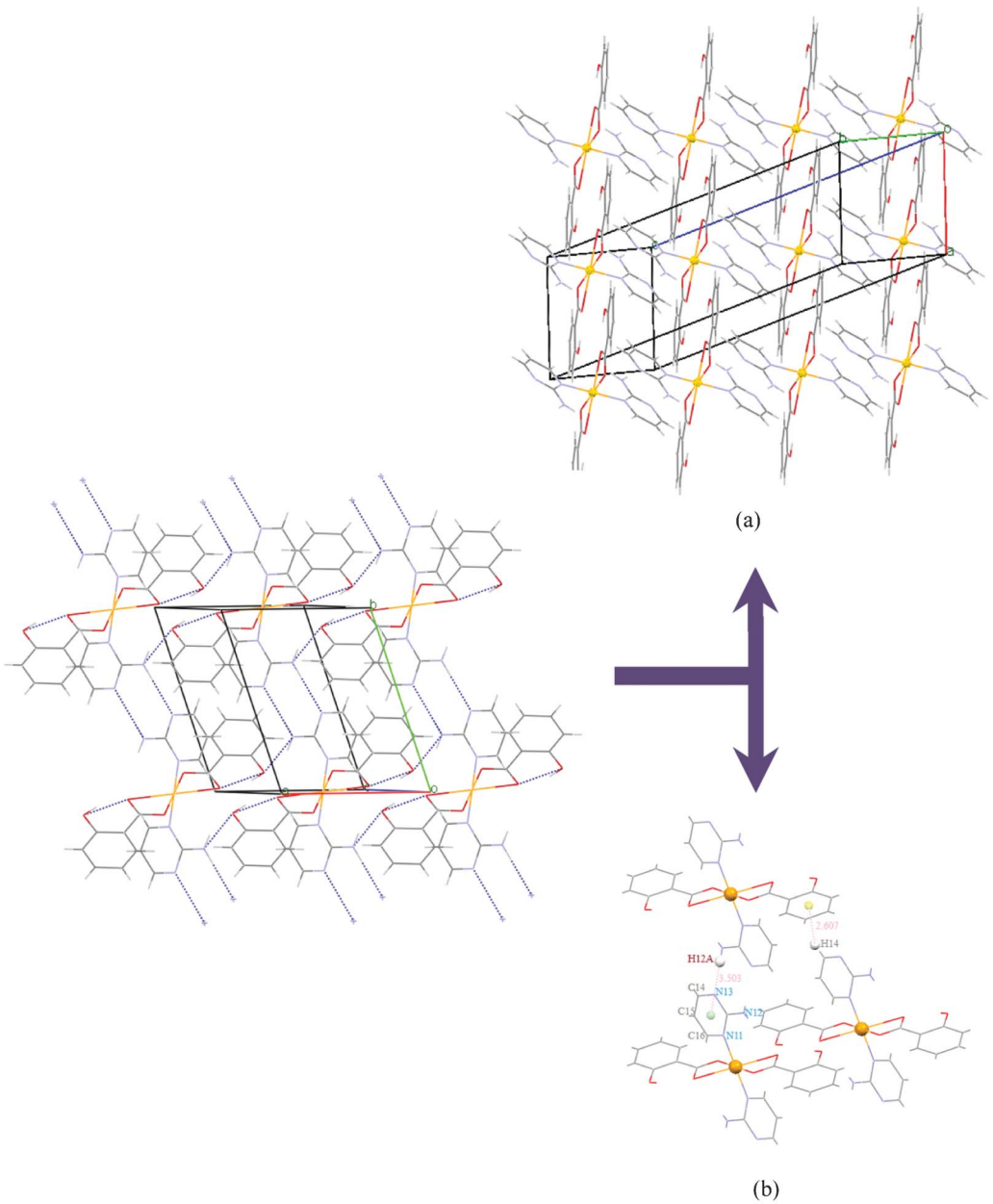

Fig. 3 A view of sheet-like in $\mathbf{I'}$ along the *ab* plane, formed *via* H-bond interactions. (a) Partial view of the arrangement of complex species (non coordinated molecules have been omitted for clarity). (b) View of two kinds of N–H···π and C–H···π interactions between adjacent species.

and stability constants of proton-transfer systems and their metal ion complexes were evaluated using BEST program described by Martell and Motekaitis.[40] The value of $K_w = [H^+][OH^-]$ used in the calculations according our previous works.[36–38]

Results and discussion

Solid-state characterization. Crystal structure of complexes

The molecular structure of **I** is shown in Fig. 1a with the atom numbering scheme. The single crystal X-ray diffraction analysis reveals that $[Cu(HSAL)_2(2\text{-apym})_2]$ crystallizes in the monoclinic system with $P2_1/n$ space group with an asymmetric unit containing one crystallographically independent Cu(II) cation, one 2-apym, and one HSAL ligand. The Cu(II) atom is coordinated by nitrogen atoms of two 2-apym ligands [Cu1–N31 = 1.998(2) Å] and four oxygen atoms from two HSAL ligands [Cu1–O1 = 1.9702(2), Cu1–O11 = 1.948(2), Cu1–O12 = 2.606(2), and Cu1–O2 = 2.523(2) Å] in which Cu1–O12 and Cu1–O2 are in axial positions affected by the Jahn–Teller distortion in the equatorial plane. Regarding bond angles in an ideal octahedral geometry, the severely distorted chelate rings within the octahedral geometry with N_2O_4Cu bounding set also demonstrate this effect. In the crystalline network of **I**, cooperation of combination of various non-covalent interactions, intra/intermolecular H-bond interactions led to the formation of one type of N–H···N homosynthon $R_2^2(8)$ besides C15–H15···π, C24–H24···π, C6–H6···π, and C16–H16···π interactions (average distances = 3.193 Å), respectively which resulted in the expansion as double chain-like architectures. In this regard, it is convenient to consider the intramolecular interaction which leads to the creation of an $S_1^1(6)$ interaction ring between coordinated carboxylate oxygens (O1 and O12) as acceptors and non-coordinated O3–H3 and O13–H13 groups belonging to HSAL ligand. This resulted in establishing a O–H···O H-bond that was cooperatively stabilized by the participation in C1=O1···π (3.846 Å) and C11=O11···π (3.691 Å) interactions. The interactions between two neighboring complexes led to a crystalline network (Fig. 2). The energies of the interactions associated with the formation of this chain-like structure will be further studied and discussed in the theoretical part. Single crystal X-ray diffraction analysis shows that compound **I′**, $[Cu(HSAL)_2(2\text{-apym})_2]\cdot(H_2SAL)_2(2\text{-apym})$, crystallizes in the triclinic system with space group $P\bar{1}$. The environment around the centrosymmetric Cu(II) complex, N_2O_4Cu bound set, can be described as the same as the coordination geometry of **I** except that **I′** comprises of intact and non-coordinated two symmetrically independent H_2SAL and one 2-apym molecules. The asymmetric unit is decorated by half of the Cu(II) complex, one 2-apym, and two symmetrically independent H_2SAL molecules (Fig. 1b). The

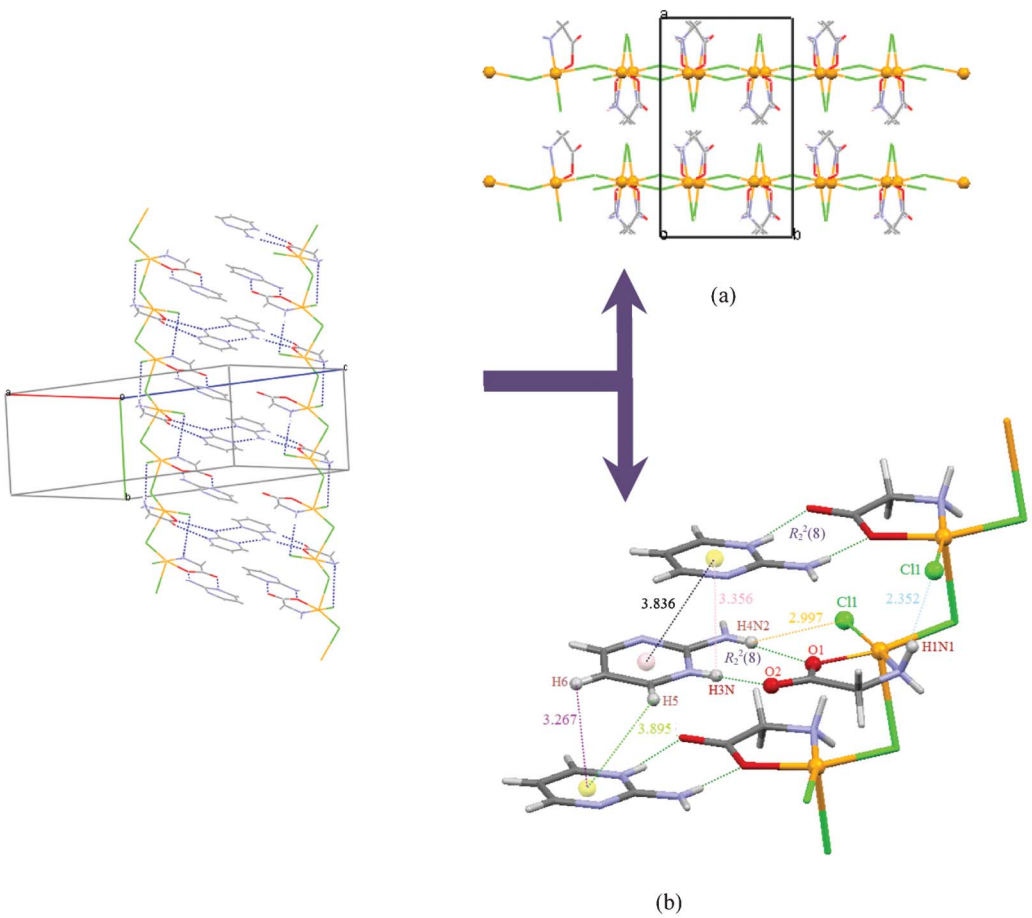

Fig. 4 A view of ladder-like in **II**, formed *via* H-bond interactions. (a) Partial view of the arrangement of complex species without non coordinated molecules. (b) View of kinds of N–H···O, π···π, N–H···π, C–H···π, and N–H···Cl interactions between adjacent species.

existent of various intermolecular H-bond interactions results in a grid-like structure of this complex (Fig. 3). Non-coordinated molecules which are well exploited in crystalline architectures contribute to generate non-flat zigzag sheets, which are connected by the carboxyl–amine and hydroxy–pyrimidine heterosynthon, [O–H···N and N–H···O, $R_2^2(8)$], finally causing formation of an acid–base motif. In our knowledge the hydrogen bond interactions by the creation of a heterosynthon as $R_6^6(34)$, besides stacking interactions between two noncoordinated 2-apym molecules, N12–H12A···π (3.503 Å), C14–H14···π (2.607 Å), N42–H42A···π (3.392 Å) and N42–H42B···π (3.743 Å) could play crucial roles in the further stabilization of **I′** (See Fig. 3). Similar to compound **I**, one can also see $S_1^1(6)$ ring interaction along with intramolecular C1=O1···π (3.698 Å) interaction. Compound **II** as a 1-D coordination polymer, $\{(H2\text{-apym})[Cu(GLY)(\mu\text{-}Cl)_2Cl]\}_n$, crystallizes in the orthorhombic system with space group *Pbca*. The crystallographic analysis indicates that the title compound consists of a discrete polymeric chain $[Cu(GLY)(\mu\text{-}Cl)_2Cl]^-$, and a cationic fragment $(H2\text{-apym})^+$. Each Cu(II) ion is surrounded by two bridged chloride ions $(\mu\text{-}Cl)_2$, one terminal Cl^-, and one GLY ligand creating chelate ring which leads to the Cu(II) centre arranged in square pyramidal fashion. The Cu–Cu distance is 3.775 Å. In the polymer, there are classical and one non-classical H-bond interactions, such as NH···Cl along with π···π stacking interactions which cause more consolidation and assemble the supramolecular network. Moreover, the carboxyl–pyrimidine hydrogen bonded synthon and pyrimidine–pyrimidine hydrogen bonded synthon form R_2^2 (8) rings. Each of the non-coordinated H2-apym cations is an effective factor to formation of these synthons *via* N3–H3N···O2, N4–H4N2···O1, and N4–H4N1···N2 H-bonds and π···π stacking interactions, leading to the supramolecular network. They play a connector role between three discrete chains by interconnecting N–HN···O and N–HN···Cl contacts. It is interesting to point out that in the title structure a rare non-classical H-bond in the form of N–HN···Cl and N–H···π stacking interaction exist, which cooperatively controls crystal growth of the structure. The chelating ring caused by coordinative N- and O- donor atoms of glycine molecules distributed in *c* direction lies alternately on opposite sides (see Fig. 4). When flexible the H_2MAL ligand was used instead of HGLY, compound **III** was formed. X-ray crystallographic data show that $[Cu(\mu\text{-}MAL)(2\text{-apym})]_n$ crystallizes in the monoclinic system with space group $P2_1/c$, and its asymmetric unit consists of one crystallographically dependent Cu(II) ion, one MAL, and one

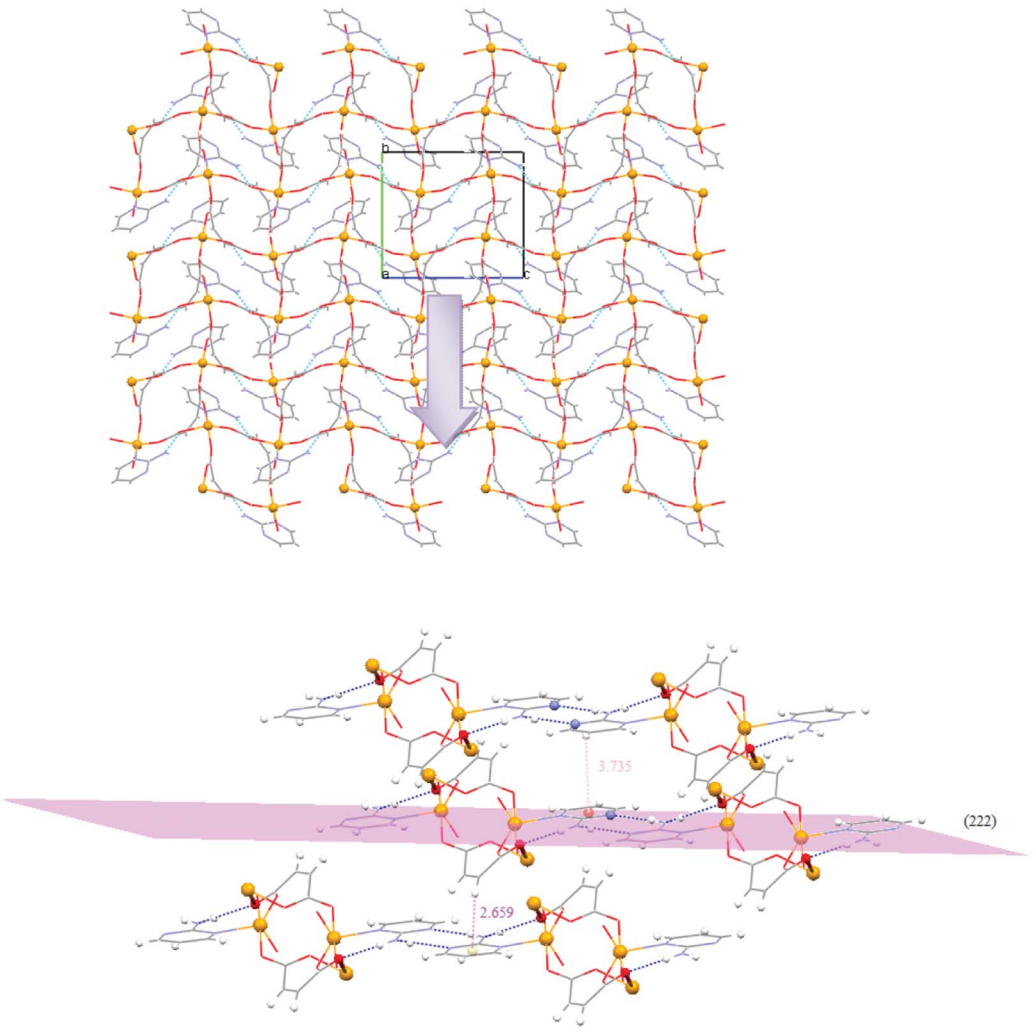

Fig. 5 (Top) A packing diagram of **III** along *ac* plane. (Bottom) Partial view of C–H···π interactions between adjacent species.

2-apym as coordinated ligands (Fig. 1d). The crystal structure of **III** reveals a 2-D coordination arrangement. Each H_2MAL ligand acts as a tridentate ligand showing μ_3-bridge mode by carboxylate groups O1–C1–O2 and O3–C3–O4 and uniform μ_2-η^1:η^1 bridging and chelating modes. As depicted in Fig. 1d, the coordination environment around the Cu(II) is portrayed as appreciably distorted NO_4Cu trigonal bipyramidal geometry. The Cu(II) is surrounded by four oxygen atoms from carboxylate groups through (O1, O3) and (O2, O4) from two symmetrically independent MAL ligands and one nitrogen atom (N11) from a coordinated 2-apym in which the Cu–O and Cu1–N11 distances range from 1.9388(16) Å to 2.562(16) Å and 2.1462(19) Å, respectively. The overall structure defines a robust intriguing 2-D architecture in which MAL ligands are considered as linkers which hinge the Cu(II) ions as nodes. Indeed, the four central fragments are further connected by two N12–H122···N13 intermolecular H-bonds in two nearly perpendicular planes related to planes of the pyrimidine ring and its amino group. These fragments create $R_2^2(8)$ homosynthon shown in the packing diagram of **III** and H-bond interactions with C–H···π in Fig. 5. It is interesting to note that 2-apym within the complex deviates from the plane (222), perhaps for steric reasons.

Network non-covalent interaction studies by DFT

Herein, the non-covalent interactions using DFT calculations have fully been considered to evaluate their binding energies governed by the crystal packing and probable interplaying of them. For all complexes the network formation energies (nfe) ($E_{nfe} = E_{network} - nE_{monomer}$) are negative, indicating the network formation with non-covalent interactions is favorable. But it should be mentioned, since there are no non-covalent interactions in formation of the compound **III** network, it has not been discussed from a theoretical point of view. Actually, this 2-D network has been expanded *via* Cu–O–C covalent bonds and finding independent monomers with connection to other ones *via* non-covalent interactions is indeed impossible. Comparison of geometrical features of these compounds shows good agreement between the optimized and experimental structures (Table 2). Various dispersive interactions, classical and non-classical H-bonds, π···π stacking, C–H···π, and N–H···π contacts stabilize the relative network of compounds **I′** and **II** (Table 4). π···π Stacking was only found in the network of compound **II** ($\mathbf{II}_{net}$). The calculated non-covalent interactions represent the following stabilization sequence: H-bond > N–H···π > C–H···π > π···π (Table 4). In compound **I**, two N_{32}–H_{32}···N_{23} (1.880 Å), two N_{22}–H_{22}···N_{33} (2.019 Å) H-bonds, and C–H···π of 2-apym with HSAL ring (2.299 Å) and *vice versa* (3.092 Å) govern formation of network of compound **I** ($\mathbf{I}_{net}$) and its fragments (**I**-fragment1, **I**-fragment2, see ESI,† Fig. 1S) (Fig. 6). The interaction energy associated with these contacts was estimated using the formation energy of the pentamer from 5 monomers, calculated to be −361.05 kcal mol^{-1}. This total energy obtained by the network is indeed the sum of the −59.73, −55.60, −46.98, and −36.42 kcal mol^{-1} for N_{32}–H_{32}···N_{23}, N_{22}–H_{22}···N_{33}, and C–H···π of 2-apym ring with HSAL and *vice versa*, respectively (Table 4). $\mathbf{I}_{net}$ contains 5 monomers ($\mathbf{I}_{mon}$) bearing all these stabilizing non-covalent interactions that participated in network formation (Fig. 6). Actually the network formation is governed by two double N–H···N H-bonds. The C–H···π stacking of HSAL with 2-apym ring and *vice versa* and N–H···N bonds show interplay with each other that causes weakness of these interactions in $\mathbf{I}_{net}$ (Fig. 6 and Fig. 1S, ESI†). The monomer of compound **I′** ($\mathbf{I'}_{mon}$) due to having two O_{32}–H_{32}···N_{42} of HSAL with 2-apym ring and *vice versa* intramolecular H-bonds (1.599 Å), four C–$H_{2\text{-apym}}$···π_{HSAL}

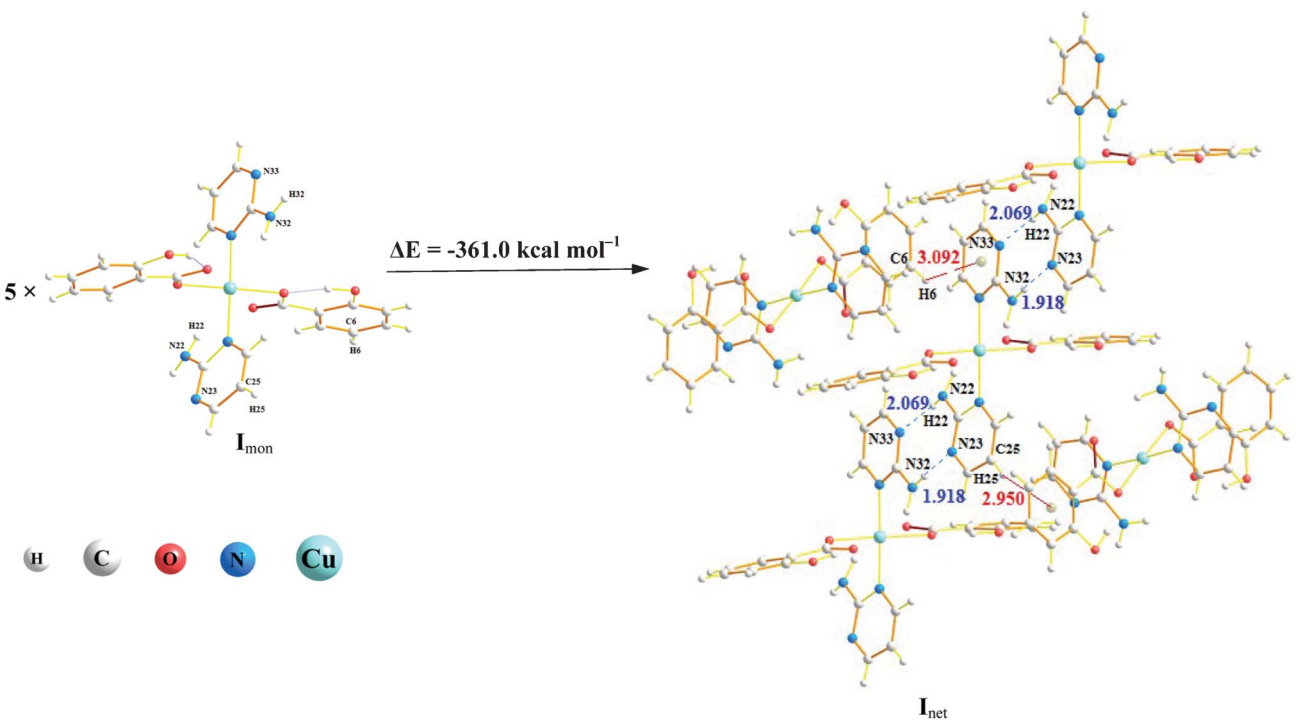

Fig. 6 Formation energy of $\mathbf{I}_{net}$ (distances are given in Å).

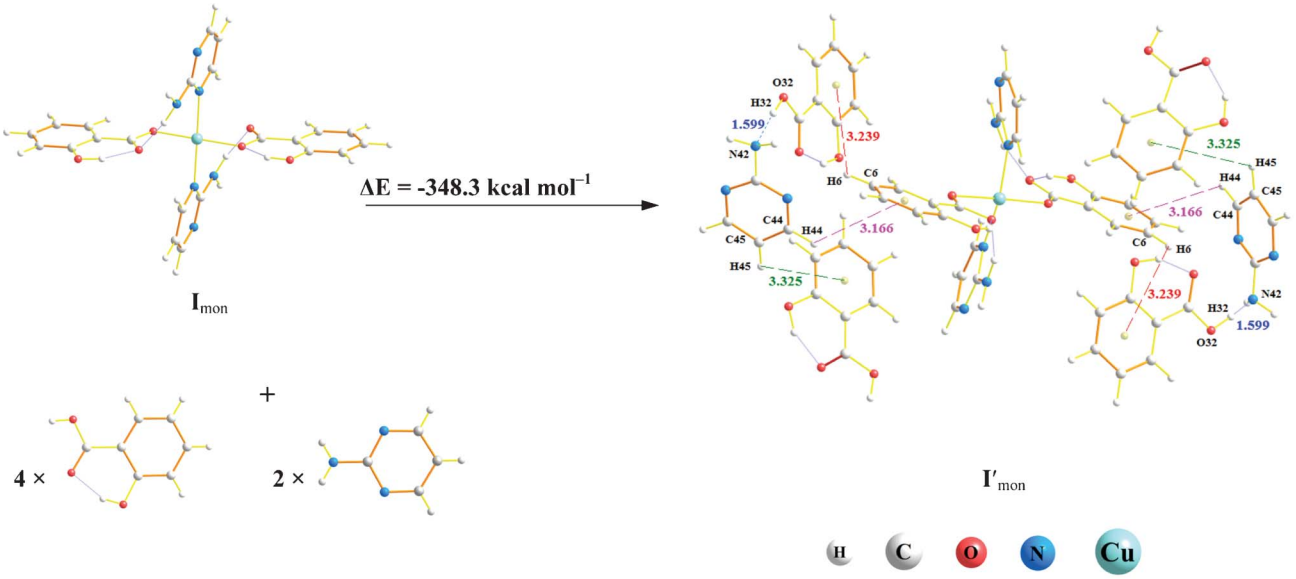

Fig. 7 Stabilization energy of $\mathbf{I}'_{mon}$ compared to $\mathbf{I}_{mon}$ (distances are given in Å).

bonds (3.325, 3.166 Å) and two C_{44}–$H_{44,HSAL}\cdots\pi_{HSAL}$ bonds (3.239 Å) stabilizes −348.26 kcal mol^{-1} more than $\mathbf{I}_{mon}$ (Fig. 7). For more clarity, here, we try to classify different types of non-covalent interactions and their binding energies among constituents of crystal lattice for stabilizing of the network of $\mathbf{I}'$ ($\mathbf{I}'_{net}$). At first, the double N–$H_{2\text{-apym}}\cdots N_{2\text{-apym}}$ (1.919 Å) H-bonds are considered, which contribute to the stabilization of $\mathbf{I}'_{net}$ in 234.0 kcal mol^{-1} (Fig. 2S, ESI†), comparable to the contribution in stabilization of **I**-fragment (Fig. 1S, ESI†). We are looking for all involved non-covalent interactions and their stabilization energies for $\mathbf{I}'_{net}$ formation. For this purpose considering all constraining parts of $\mathbf{I}'_{mon}$ is not avoidable. In the next step, two 2-apym molecules of $\mathbf{I}'_{mon}$ are considered, demonstrating they participate with two other 2-apym and four HSAL molecules in the stabilization of $\mathbf{I}'$-fragment2 (Fig. 3S, ESI†). In this system two sets of double O–$H_{HSAL}\cdots N_{2\text{-apym}}$ (1.582,

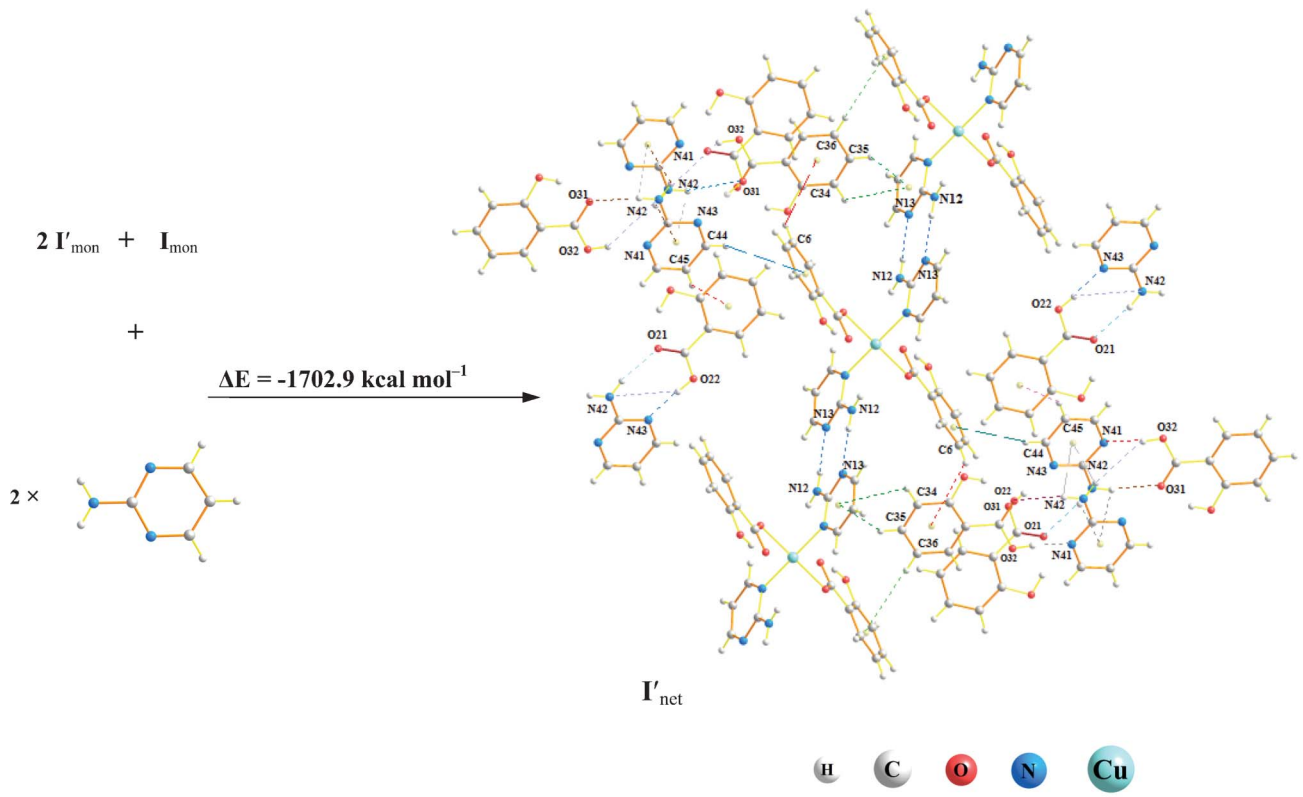

Fig. 8 Formation energies of $\mathbf{I}'_{net}$ (Å).

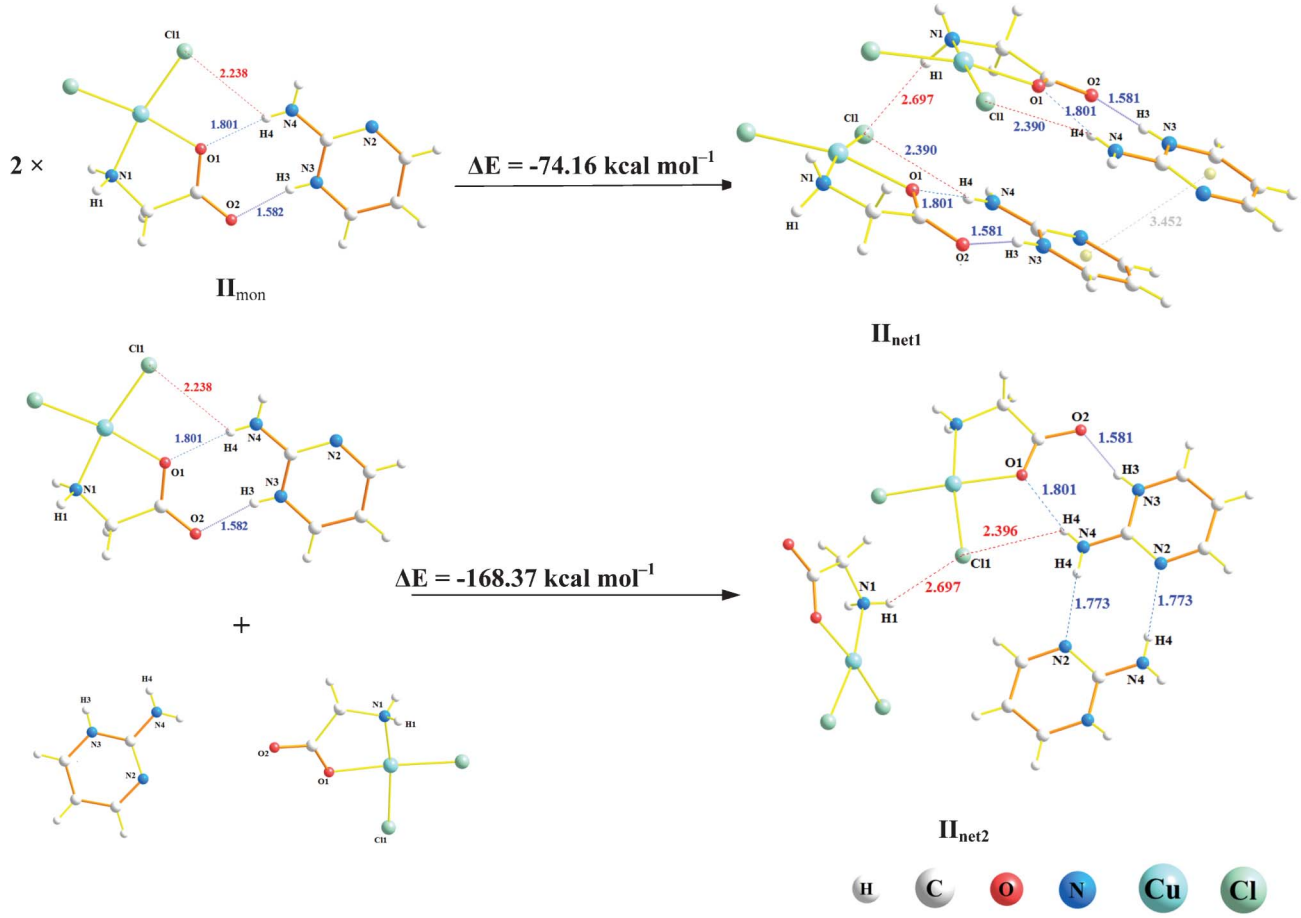

Fig. 9 Formation energies of $\mathbf{II}_{net1}$ (top) and $\mathbf{II}_{net2}$ (bottom) (distances are given in Å).

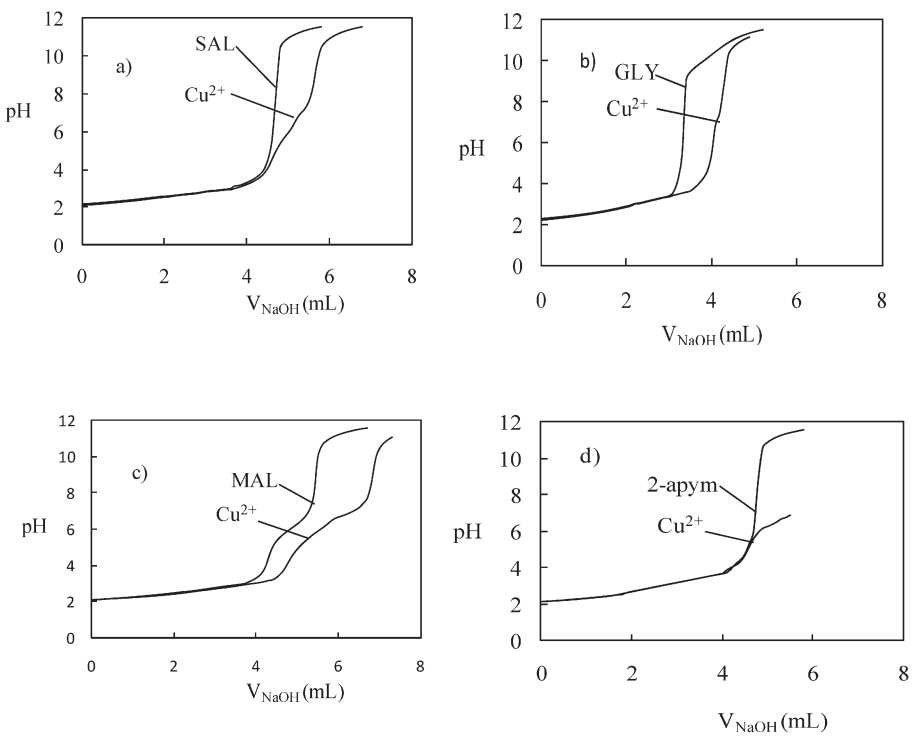

Fig. 10 Potentiometric titration curves of SAL (a), GLY (b), MAL (c) and 2-apym (d) in the absence and presence of Cu^{2+} ion with NaOH 0.09300 M in aqueous solution at 25 ± 0.1 °C and μ = 0.1 M $NaNO_3$.

Table 5 Overall stability and stepwise protonation constants of SAL, GLY, MAL and 2-apym and recognition constants for interaction between SAL/GLY/MAL and 2-apym in aqueous solution at 25 ± 0.1 °C and μ = 0.1 M $NaNO_3$

Stoichiometry	System					logβ	Equilibrium quotient	log$K$	Maximum%	pH
	2-apym	SAL	GLY	MAL	H					
SAL/2-apym	0	1	0	0	1	13.22		13.22	100.0	>5.0
	0	1	0	0	2	16.08		2.86	90.40	2.0
	1	0	0	0	1	3.39		3.39	96.08	2.0
	1	1	0	0	1	16.40	[2-apymSALH]/[2-apym][SALH]	3.18	58.36	>4.6
	1	1	0	0	3	22.85	[2-apym$SALH_3$]/[2-apymH][$SALH_2$]	3.38	62.45	2.0
GLY/2-apym	0	0	1	0	1	10.22		10.2	99.96	4.7–8.2
	0	0	1	0	2	12.89		2.67	82.12	2.0
	1	0	1	0	1	13.91	[2-apymGLYH]/[2-apym][GLYH]	3.69	75.16	4.4–9.9
	1	0	1	0	2	17.07	[2-apym$GLYH_2$]/[2-apymH][GLYH]	3.46	30.1	3.0
							[2-apym$GLYH_2$]/[2-apym][$GLYH_2$]	4.18		
	1	0	1	0	3	19.90	[2-apym$GLYH_3$]/[2-apymH][$GLYH_2$]	3.62	62.36	2.0
MAL/2-apym	0	0	0	1	1	5.98		5.98	96.76	4.2
	0	0	0	1	2	8.40		2.42	72.68	2.0
	1	0	0	1	1	9.94	[2-apymMALH]/[2-apym][MALH]	3.96	80.36	4.1–5.6
							[2-apymMALH]/[2-apymH][MAL]	6.55		
	0	0	0	1	3	15.08	[2-apym$MALH_3$]/[2-apymH][$MALH_2$]	3.29	55.72	2.0

1.599 Å), four N–$H_{2\text{-apym}}$ ···O_{HSAL} (1.993 Å), two C–$H_{2\text{-apym}}$···π_{HSAL} (3.166 Å), and four sets of double N–$H_{2\text{-apym}}$···$\pi_{2\text{-apym}}$ (3.053, 3.430 Å) govern the formation of **I**′-fragment2 (Fig. 3S, ESI†, Table 4). In the last step, addition of the remaining parts of $\mathbf{I}'_{mon}$ (two HSAL molecules) to **I**′-fragment2 causes to involve two more 2-apym and two more HSAL molecules exhibiting two O–H_{HSAL}···$N_{2\text{-apym}}$ (1.607 Å), two N–$H_{2\text{-apym}}$···O_{HSAL} (1.887 Å), four sets of double C–H_{HSAL}···$\pi_{2\text{-apym}}$ (3.047, 3.093, 3.151 and 3.239 Å), and two C–$H_{2\text{-apym}}$···π_{HSAL} (3.325 Å) for stabilization of $\mathbf{I}'_{net}$ (Fig. 8 and Fig. 4S, ESI†). The formation energy of $\mathbf{I}'_{net}$ trimer associated with all of these contacts (−1702.9 kcal mol^{-1}) has been estimated through similar route used for compound **I**. The calculated interaction energies show that near three fifths (−1002.7 kcal mol^{-1}) of network stabilization energy comes from H-bonds (Table 4). For compound **II**, species $\mathbf{II}_{mon}$ as selected monomer was employed for starting calculations (Fig. 9). In

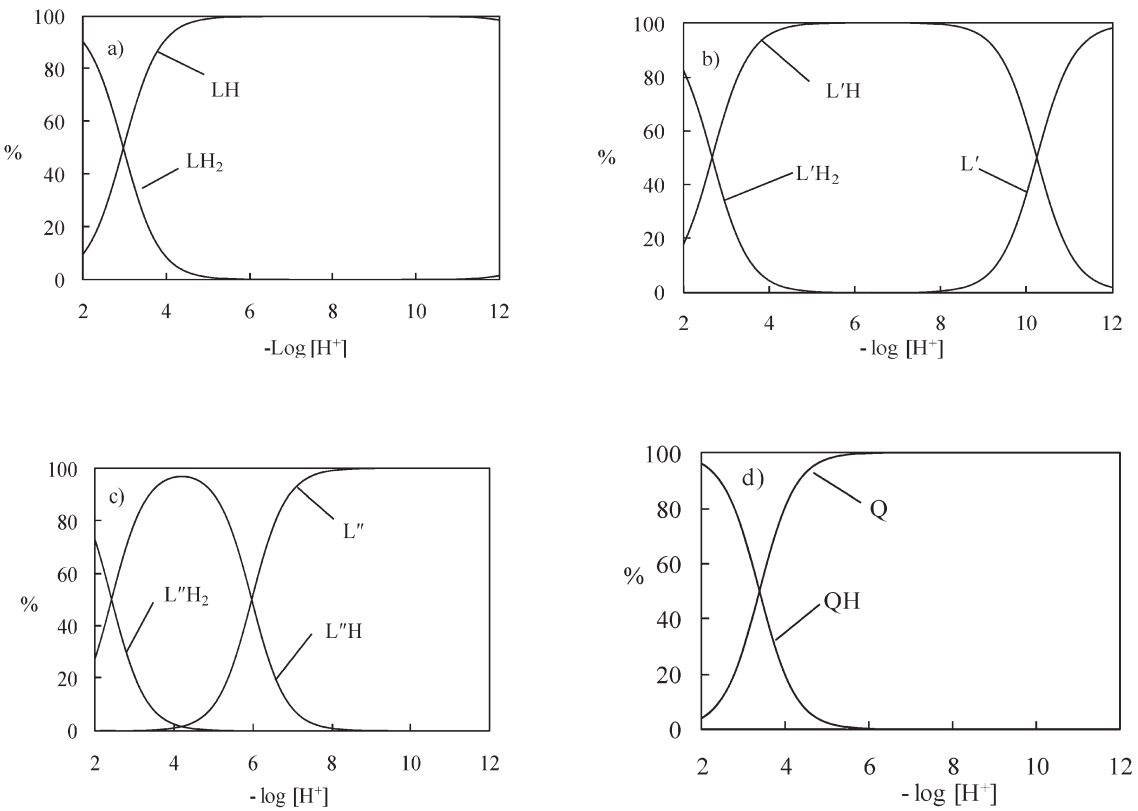

Fig. 11 Distribution diagrams of SAL(L) (a), GLY(L′) (b), MAL(L″) (c) and 2-apym (Q) (d).

this inner-sphere complex, N_3–H_3···O_2 (1.582 Å) and N_4–H_4···O_1 (1.801 Å) intramolecular interactions stabilize its conformation in the solid state. Paying attention to different non-covalent interactions of the network of compound **II**, we could choose two species (**II**$_{net1}$, **II**$_{net2}$, Fig. 9). Comparing to **II**$_{mon}$, for **II**$_{net1}$, $\pi_{2\text{-apym}}$···$\pi_{2\text{-apym}}$ stacking (3.452 Å), and N_1–H_1···Cl_1 non-classical H-bond (2.697 Å) and for **II**$_{net2}$, non-classical N_1–H_1···Cl_1 (2.697 Å), and double N_4–H_4···N_2 (1.773 Å) H-bonds cause −74.16 and −168.37 kcal mol^{-1} stabilization energy, respectively (Table 4). The title π···π interaction results in a N–centroid$_{2\text{-apym}}$ distance of 3.452 Å which reflects a moderate interaction of the N atom of the top ring with the π cloud of bottom ring and *vice versa* (indeed a strong interaction is characterized by a separation distance below 3.03 Å).[41] Comparing **II**$_{net1}$ and **II**$_{net2}$ (Fig. 9) indicates that the N_1–H_1···Cl_1 bond displayed a little interplaying on N_4–H_4···Cl_1, which causes weakness of the latter in **II**$_{net2}$. For compound **II** some weak and not real non-covalent contacts (N_2–H_1···Cl_2, 2.984 Å, N_1–H_1···Cl_2, 3.042 Å) having no important effect in related network formation are not considered in the theoretical point of view. Generally, the comparison of all of these H-bond and stacking non-covalent interaction distances show stabilization order as: O–H···N > N–H···O > N–H···N > N–H···Cl > C–H···π > N–H···π > π···π (Table 4). It is noteworthy to say that the energy values reported in this work have good agreement with experimental data similar to the previously reported theoretical research in literature.[42]

Solution studies

In this section primarily, the fully protonated forms of SAL(L), GLY(L′), MAL(L′′) and 2-apym(Q) were titrated with a standard NaOH solution (Fig. 10a–d) in order to obtain their protonation constants as the building blocks of the SAL/2-apym, GLY/2-apym, MAL/2-apym adducts. The protonation constants of SAL, GLY, MAL and 2-apym were calculated by fitting the volume–pH data to BEST program. The results are summarized in Table 5. It is noteworthy that the resulting protonation constant values are in satisfactory agreement with those reported in the literature.[43–46] Distribution diagrams for all ligands are shown in Fig. 11a–d. The evaluation of the equilibrium constants for the interaction of SAL/GLY/MAL with 2-apym in different protonation forms was accomplished through comparison of the calculated and experimental pH profiles obtained with SAL/2-apym, GLY/2-apym or MAL/2-apym present.[36,47,48] The results are shown in Table 5. The corresponding species distribution diagrams for SAL/2-apym, GLY/2-apym, MAL/2-apym are shown in Fig. 12a–c. The binding constants for the binary species formed from SAL/2-apym, GLY/2-apym and MAL/2-apym are listed in Table 5. The most abundant proton-transfer species for SAL/2-apym present at pH > 4.6 (58.36%) and 2.0 (62.45%) are: [2-apym][HSAL] (log$K$ = 3.18) and [H2-apym][H_2SAL] (log$K$ = 3.38); for GLY/2-apym present at pH 4.4–9.9 (75.16%), 3.0 (30.1%) and 2.0 (62.36) are: [2-apym][HGLY] (log$K$ = 3.69), {[H2-apym][HGLY](log$K$ = 3.46),

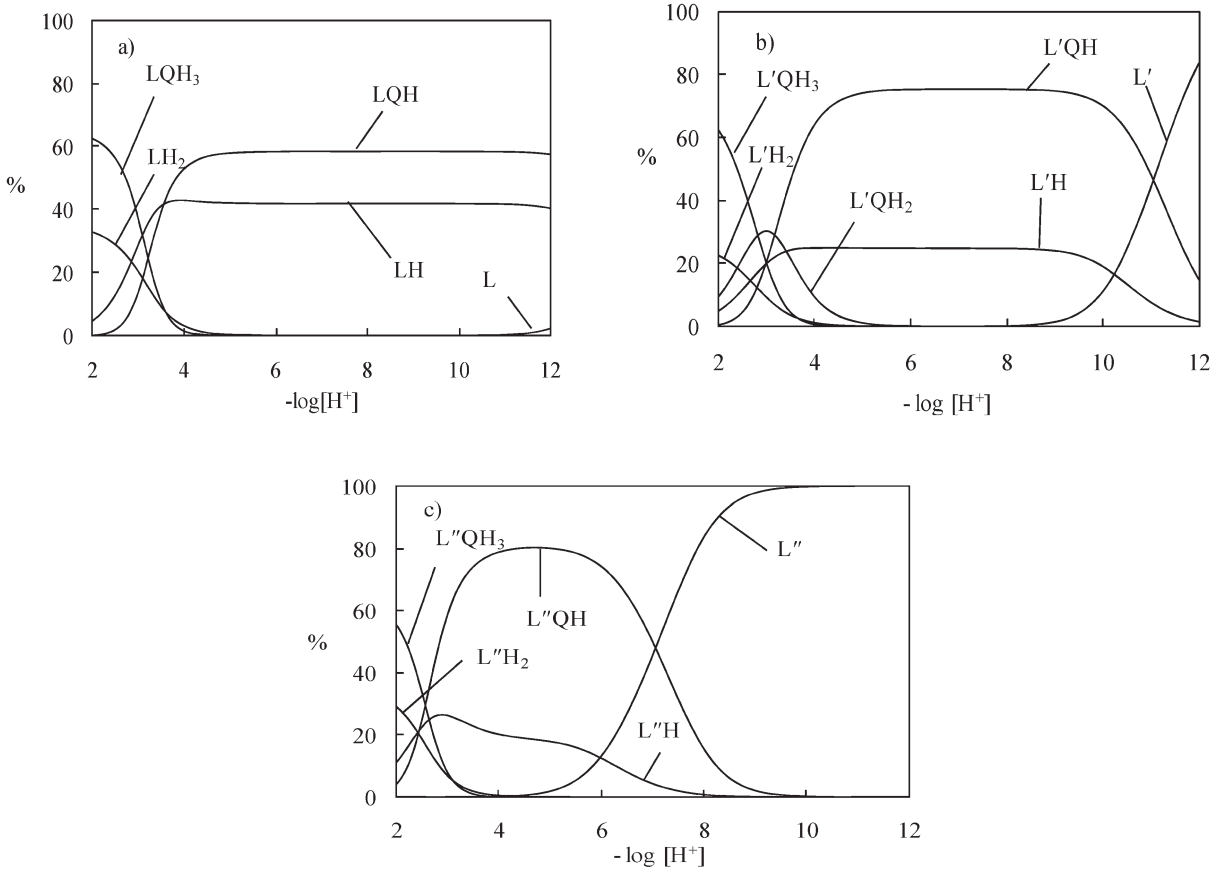

Fig. 12 Distribution diagrams for the proton-transfer interaction between SAL(L)/2-apym(Q) (a), GLY(L′)/2-apym(Q) (b) and MAL(L′′)/2-apym(Q) (c) in all probability protonated forms.

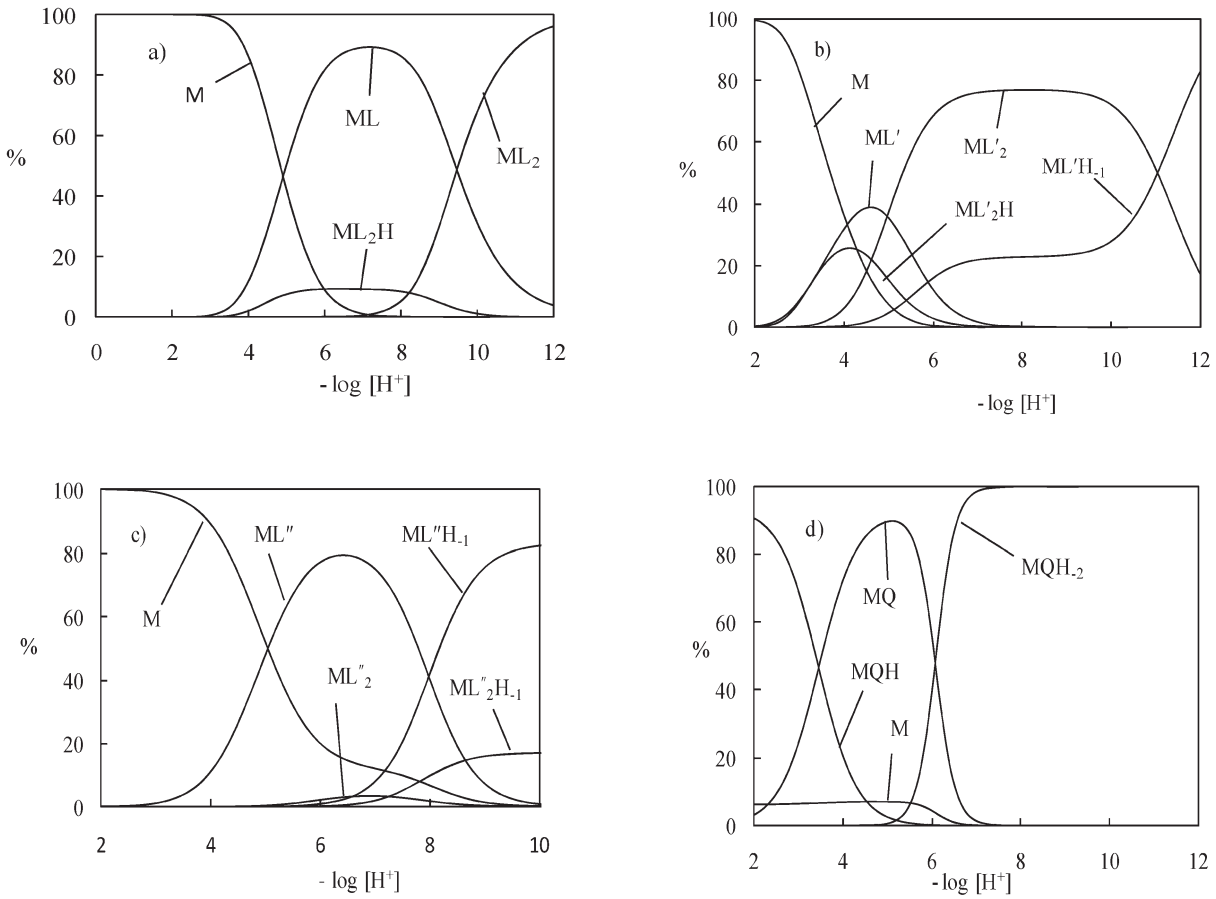

Fig. 13 Distribution diagrams of M/SAL(L) (a), M/GLY(L′) (b), M/MAL(L′′) (c) and M/2-apym (Q) (d) binary systems M=Cu^{2+}.

[2-apym][H_2GLY] (log$K$ = 4.18)} and [H2-apym][H_2GLY] (log$K$ = 3.62); for MAL/2-apym present at pH 4.1–5.6 (80.36%) and 2.0 (55.72%) are: {[2-apym][HMAL] (log$K$ = 3.96), [H2-apym][MAL] (log$K$ = 6.55)} and [H2-apym][H_2MAL] (log$K$ = 3.29). In order to evaluate the stoichiometry and stability of Cu^{2+} ion complexes with SAL/2-apym, GLY/2-apym and MAL/2-apym proton-transfer systems in aqueous solution, the equilibrium potentiometric pH titration profiles of SAL, GLY, MAL, 2-apym and their 1 : 1 mixture were obtained in the absence and presence of the Cu^{2+} ion. The resulting pH profiles are shown in Fig. 10a–d and Fig. 14 (a–c). It is seen from Fig. 10d that the titration of 2-apym in the presence of Cu^{2+} ion was stopped when the formation of precipitate in solution was observed. It was found that 2-apym forms weak complexes with the Cu^{2+} ion and the potentiometric titration curves SAL/2-apym, GLY/2-apym and MAL/2-apym mixtures are depressed considerably in the presence of the cited metal ion. The results are shown in Table 6. The calculated values are in agreement with previous reports.[45,49,50] The cumulative stability constants of $M_mL_lQ_qH_h$, β_{mlqh}, are defined in our previous publications.[36,37] They are M, L (L′, L′′), Q and H as metal ion, SAL (GLY, MAL), 2-apym and proton, respectively, and m, l, q and h are the respective stoichiometric coefficients. The cumulative stability constants were evaluated by fitting the corresponding pH–volume data to BEST program and the resulting values for the most likely complexed species in aqueous solutions are also included in Table 6 and the corresponding distribution diagrams are shown in Fig. 13a–d and 15a–c. These results revealed that the Cu^{2+} ions form relatively stable

Table 6 Overall stability constants of 2-apym/SAL, GLY or MAL/Cu (Q/L, L′ or L′′/M) binary and ternary systems in aqueous solution at 25 ± 0.1 °C and μ = 0.1 M $NaNO_3$

System	M	L	L′	L′′	Q	H	logβ	Maximum %	pH
Cu/2-apym	1	0	0	0	1	0	3.98	89.76	5.1
	1	0	0	0	1	1	7.12	90.4	2.0
	1	0	0	0	1	−2	−8.17	100.0	>7.8
Cu/SAL	1	1	0	0	0	0	10.94	89.2	6.7–7.7
	1	2	0	0	0	0	17.78	96.16	12.0
	1	2	0	0	0	1	25.28	9.36	5.6–7.6
Cu/GLY	1	0	1	0	0	0	9.07	38.81	4.6
	1	0	2	0	0	0	17.48	77.06	6.5–9.7
	1	0	2	0	0	1	22.10	25.64	4.1
	1	0	1	0	0	−1	3.18	82.96	12.0
Cu/MAL	1	0	0	1	0	0	3.71	79.18	6.4
	1	0	0	2	0	0	5.29	3.50	6.5–7.3
	1	0	0	1	0	−1	−4.27	82.96	11.3–12
	1	0	0	2	0	−1	−1.97	17.03	10.5–12.0
Cu/SAL/2-apym	1	1	0	0	1	1	19.73	8.75	2.9–3.9
	1	2	0	0	2	1	33.98	26.78	7.2
	1	2	0	0	2	2	40.79	70.43	4.2–5.2
Cu/GLY/2-apym	1	0	1	0	1	0	13.23	39.52	5.4
	1	0	1	0	1	1	16.67	26.8	3.7
Cu/MAL/2-apym	1	0	0	1	1	0	14.09	90.64	4.5–5.5
	1	0	0	1	1	2	17.10	77.86	2.1

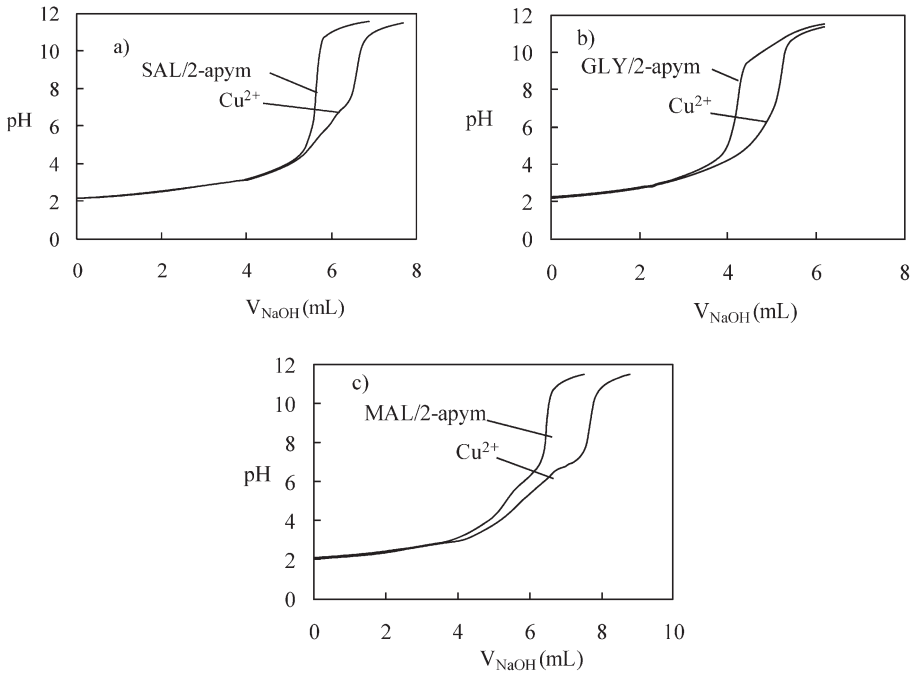

Fig. 14 Potentiometric titration curves of SAL/2-apym (a), GLY/2-apym (b) and MAL/2-apym(c) in the absence and presence of Cu^{2+} ion with NaOH 0.09300 M in aqueous solution at 25 ± 0.1 °C and μ = 0.1 M $NaNO_3$.

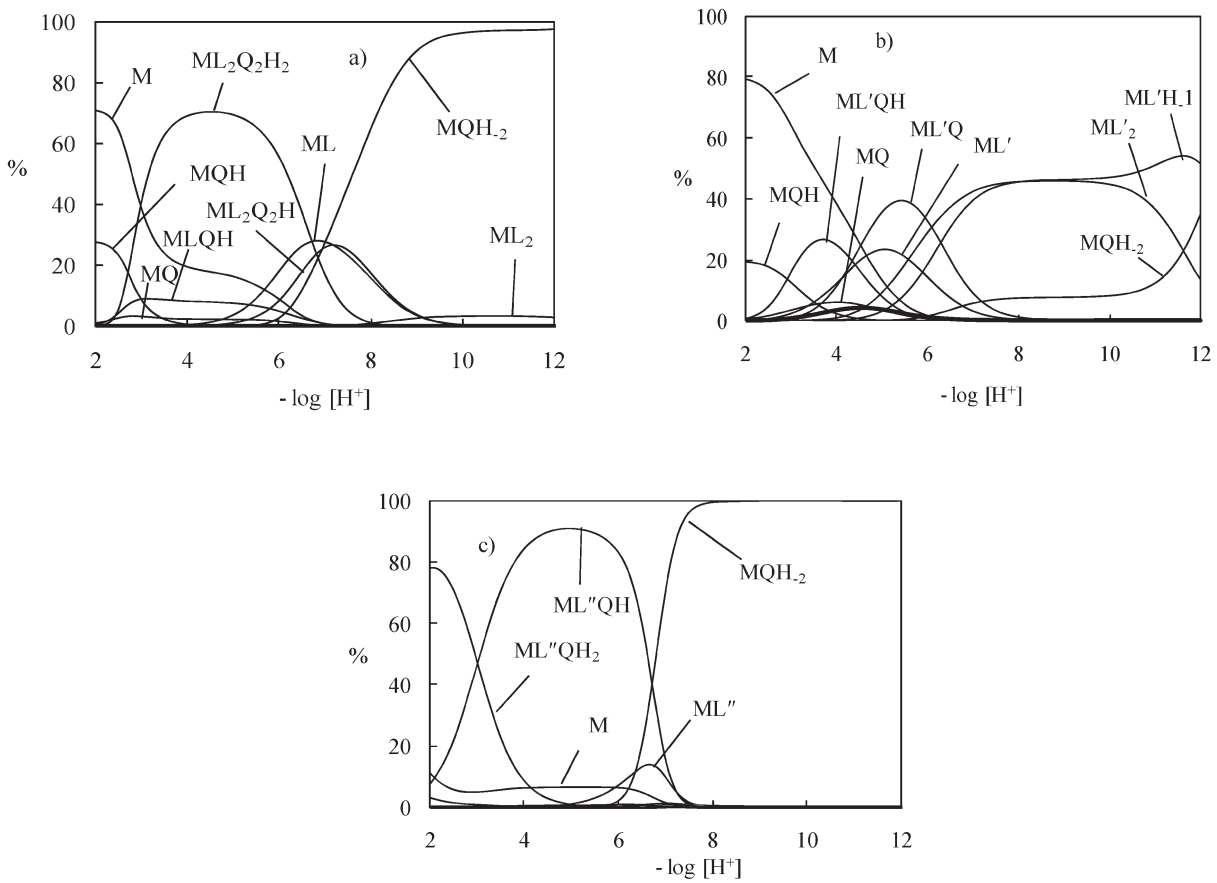

Fig. 15 Distribution diagrams of M/SAL(L)/2-apym (Q) (a), M/GLY(L′)/2-apym(Q) (b) and M/MAL(L′′)/2-apym(Q) (c) ternary systems M = Cu^{2+}.

complexes with SAL, GLY, MAL alone and mixed with 2-apym, including SAL/2-apym, GLY/2-apym and MAL/2-apym systems, but weak complexes with 2-apym. Fig. 13a–c and Table 6 show for Cu/2-apym/SAL/GLY/MAL binary systems, the most likely species are: CuQ, CuQH, $CuQH_{-2}$, CuL, CuL_2, CuL_2H, CuL′, CuL'_2, CuL'_2H, $CuL'H_{-1}$, CuL″, CuL''_2, $CuL''H_{-1}$ and CuL''_2H_{-1}. Fig. 15a–c and Table 6 revealed the formation of a variety of ternary complexes between the Cu^{2+} ion and the cited proton-transfer systems at different ranges of pH. The predominant species for Cu/SAL/2-apym are: CuLQH (at pH 2.9–3.9), CuL_2Q_2H (at pH 7.2) and $CuL_2Q_2H_2$ (at pH 4.2–5.2), for Cu/GLY/2-apym are: CuL′Q (at pH 5.4) and CuL′QH (at pH 3.7), for Cu/MAL/2-apym are: CuL″QH (at pH 4.5–5.5) and $CuL''QH_2$ (at pH 2.1). The stoichiometries of the some of the most abundant ternary complexes such as $ML_2Q_2H_2$, ML′QH, ML″QH and $ML''QH_2$ existing in aqueous solution are very similar to those reported for the corresponding isolated complexes in the solid state. It should be pointed out that the complex formation is significantly affected by the pH value of the reaction system. All ligands are proton-acid or bases, and the reactions of them generate HCl as a by-product. The pH value of each reaction mixture would be informative for the understanding the relationship between the pH value and the components of resulting products.

Conclusion

Understanding of the essential roles of non-covalent interactions in network formation as their stabilization energies could be useful tools for designing new desired ligands within crystal engineering. For this purpose, the smallest structure of networks of compounds **I**, **I′**, and **II** containing a number of respective monomers bearing all possible non-covalent interactions as input files have been chosen. It should be pointed out that accurate selection of these monomers for starting theoretical calculations have essential contributions for better fitness of theoretical outputs of structural parameters with the experimental ones. Different non-covalent interactions, with the stabilization sequence of H-bond > C–H···π > N–H···π > π···π have been found in the title networks. $\mathbf{I}_{net}$ and $\mathbf{I}'_{net}$ contain 5 and 3 respective monomer respectively, bearing N–H···N, N–H···O and O–H···N H-bonds, C–H···π, and N–H···π interactions. For compounds **II** two networks ($\mathbf{II}_{net1}$ and $\mathbf{II}_{net2}$) contain 2 monomers bearing N–H···Cl and N–H···N H-bonds, and π···π interactions have been found. The calculated binding energies of these non-covalent interactions indicated classical H-bonds play the most important role in the network stabilization. The protonation constants of SAL, GLY, MAL and 2-apym, the building blocks of the proton-transfer systems including SAL/2-apym, GLY/2-apym and MAL/2-apym fragments, and the corresponding stability constants of these systems were determined by potentiometric study. Comparison of the proton-transfer stability constants for the three proton-transfer systems described reveals that the almost similar tendency between them. Also these systems form stable complexes with Cu^{2+} ion.

Acknowledgements

The authors gratefully acknowledge the financial support by the Ferdowsi University of Mashhad, Mashhad, Iran. We also thank the computing centre of the Friedrich-Schiller Universität Jena (URZ), Jena, Germany for supplying their Cray XD1 (officer: Sabine Irmer) for performing the computational research part.

References

1 J. D. van der Waals, *PhD thesis*, University of Leiden, Leiden, The Netherlands, 1873.
2 G. A. Jeffrey and W. Saenger, *Hydrogen Bonding in Biological Structures*, Springer-Verlag, Berlin, 1991.
3 (*a*) R. A. Kumpf and D. A. Dougherty, *Science*, 1993, **261**, 1708; (*b*) L. Heginbotham, Z. Lu, T. Abramson and R. Mackinnon, *Biophys. J.*, 1994, **66**, 1061.
4 (*a*) S. Demeshko, S. Dechert and F. Meyer, *J. Am. Chem. Soc.*, 2004, **126**, 4508; (*b*) B. L. Schottel, J. Bacsa and K. R. Dunbar, *Chem. Commun.*, 2005, 46; (*c*) Y. S. Rosokha, S. V. Lindeman, S. V. Rosokha and J. K. Kochi, *Angew. Chem., Int. Ed.*, 2004, **43**, 4650; (*d*) P. de Hoog, P. Gamez, I. Mutikainen, U. Turpeinen and J. Reedijk, *Angew. Chem., Int. Ed.*, 2004, **43**, 5815; (*e*) A. Frontera, F. Saczewski, M. Gdaniec, E. Dziemidowicz-Borys, A. Kurland, P. M. Deya, D. Quiñonero and C. Garau, *Chem.–Eur. J.*, 2005, **11**, 6560; (*f*) G. Gil-Ramirez, J. Benet-Buchholz, E. C. Escudero-Adan and P. Ballester, *J. Am. Chem. Soc.*, 2007, **129**, 3820.
5 R. Bhattacharyya, U. Samanta and P. Chakrabarti, *Protein Eng.*, 2002, **15**, 91 and references therein.
6 G. R. Desiraju, *Angew. Chem., Int. Ed. Engl.*, 1995, **34**, 2311.
7 K. Müller-Dethlefs and P. Hobza, *Chem. Rev.*, 2000, **100**, 143.
8 K. E. Riley, M. Pitoňák, P. Jurečka and P. Hobza, *Chem. Rev.*, 2010, **110**, 5023.
9 B. Moulton and M. J. Zaworotko, *Chem. Rev.*, 2001, **101**, 1629.
10 A. M. Shultz, O. K. Farha, J. T. Hupp and S. T. Nguyen, *J. Am. Chem. Soc.*, 2009, **131**, 4204.
11 O. M. Yaghi, M. ÓKeeffe, N. W. Ockwig, H. K. Chae, M. Eddaoudi and J. Kim, *Nature*, 2003, **423**, 705.
12 S. Kitagawa and K. Uemura, *Chem. Soc. Rev.*, 2005, **34**, 109.
13 X. M. Chen and M. L. Tong, *Acc. Chem. Res.*, 2007, **40**, 162.
14 B. Zhang, D. Zhu and Y. Zhang, *Chem.–Eur. J.*, 2010, **16**, 9994.
15 W. Wei, M. Wu, Q. Gao, Q. Zhang, Y. Huang, F. Jiang and M. Hong, *Inorg. Chem.*, 2009, **48**, 420.
16 L. A. Barrios, G. Aromí, A. Frontera, D. Quiñonero, P. M. Deyà, P. Gamez, O. Roubeau, E. J. Shotton and J. S. Teat, *Inorg. Chem.*, 2008, **47**, 5873.
17 C. A. Black, L. R. Hanton and M. D. Spicer, *Inorg. Chem.*, 2007, **46**, 3669.
18 H. Chun and J. Seo, *Inorg. Chem.*, 2009, **48**, 9980.
19 H. Chun and N. Jin, *Bull. Korean Chem. Soc.*, 2009, **30**, 1405.
20 G. Yang, H.-G. B.-H. Zhu and X.-M. L. Chen, *J. Chem. Soc., Dalton Trans.*, 2001, 580.
21 Z.-P. Deng, L.-H. Huo, M.-S. Li, L.-W. Zhang, Z.-B. Zhu, H. Zhao and S. Gao, *Cryst. Growth Des.*, 2011, **11**, 3090.
22 (*a*) M. Mirzaei, H. Aghabozorg and H. Eshtiagh-Hosseini, *J. Iran. Chem. Soc.*, 2011, **8**, 580 and references therein; (*b*) M. Mirzaei, H. Eshtiagh-Hosseini, A. Hassanpoor, T. Szymańska-Buzar, J. T. Mague, M. Korabik and A. Kochel, *Inorg. Chim. Acta*, 2012, **391**, 232.
23 Z.-L. Xu, Y. He, S. Ma and X.-Y. Wang, *Transition Met. Chem.*, 2011, **36**, 585.
24 G. R. Desiraju, *Nature*, 2001, **412**, 397.
25 L. Bolundut, I. Haiduc, E. Ilyes, G. Kociok-Köhn, K. C. Molloy and S. Gómez-Ruiz, *Inorg. Chim. Acta*, 2010, **363**, 4319.
26 A. Moghimi, R. Alizadeh, A. Shokrollahi, H. Aghabozorg, M. Shamsipur and A. Shockravi, *Inorg. Chem.*, 2003, **42**, 1616.
27 K. Müller-Dethlefs and P. Hobza, *Chem. Rev.*, 2000, **100**, 143.
28 (*a*) Bruker, *APEX II software package, v. 1.27, Bruker molecular analysis research tool*, Bruker AXS, Madison, WI, 2005; (*b*) Stoe & Cie, *X-AREA*, Stoe & Cie, Darmstadt, Germany, 2005; (*c*) G. M. Sheldrick, *Acta Crystallogr., Sect. A: Fundam. Crystallogr.*, 2008, **64**, 112; (*d*) G. M. Sheldrick, *SADABS, v. 2.03, Bruker/Siemens area detector absorption correction program*. Bruker AXS, Madison, 2003; (*e*) Bruker, *SAINT, v. 6.2, Data reduction and correction program*, Bruker AXS, Madison, 2001; (*f*) G. M. Sheldrick, *SHELXTL, v. 6.12, Structure determination software suite*, Bruker AXS, Madison, 2001.
29 M. J. Frisch, G. W. Trucks, H. B. Schlegel, G. E. Scuseria, M. A. Robb, J. R. Cheeseman, G. Scalmani, V. Barone, B. Mennucci, G. A. Petersson, H. Nakatsuji, M. Caricato, X. Li, H. P. Hratchian, A. F. Izmaylov, J. Bloino, G. Zheng, J. L. Sonnenberg, M. Hada, M.

Ehara, K. Toyota, R. Fukuda, J. Hasegawa, M. Ishida, T. Nakajima, Y. Honda, O. Kitao, H. Nakai, T. Vreven, J. A. Montgomery, Jr., J. E. Peralta, F. Ogliaro, M. Bearpark, J. J. Heyd, E. Brothers, K. N. Kudin, V. N. Staroverov, R. Kobayashi, J. Normand, K. Raghavachari, A. Rendell, J. C. Burant, S. S. Iyengar, J. Tomasi, M. Cossi, N. Rega, J. M. Millam, M. Klene, J. E. Knox, J. B. Cross, V. Bakken, C. Adamo, J. Jaramillo, R. Gomperts, R. E. Stratmann, O. Yazyev, A. J. Austin, R. Cammi, C. Pomelli, J. Ochterski, R. L. Martin, K. Morokuma, V. G. Zakrzewski, G. A. Voth, P. Salvador, J. J. Dannenberg, S. Dapprich, A. D. Daniels, O. Farkas, J. B. Foresman, J. V. Ortiz, J. Cioslowski and D. J. Fox, *GAUSSIAN 09 (Revision A.2)*, Gaussian, Inc., Wallingford, CT, 2009.

30 C. Lee, R. G. Parr and W. Yang, *Phys. Rev. B*, 1988, **37**, 785.

31 A. D. Becke, *J. Chem. Phys.*, 1993, **98**, 5648.

32 A. D. Becke, *Phys. Rev. A*, 1988, **38**, 3098.

33 (*a*) J. E. D. Bene, W. B. Person and K. Szczepaniak, *J. Phys. Chem.*, 1995, **99**, 10705; (*b*) J. Florián and B. G. Johnson, *J. Phys. Chem.*, 1995, **99**, 5899; (*c*) J. E. Combarida and N. R. Kestner, *J. Phys. Chem.*, 1995, **95**, 2717; (*d*) C. Lee, C. Sosa, M. Planas and J. J. Novoa, *J. Chem. Phys.*, 1996, **104**, 7081.

34 S. B. Boys and F. Bernardi, *Mol. Phys.*, 1970, **19**, 553.

35 P. Jurecka, J. Cerny, P. Hobza and D. R. Salahub, *J. Comput. Chem.*, 2007, **28**, 555.

36 M. Mirzaei, H. Eshtiagh-Hosseini, V. Lippolis, H. Aghabozorg, D. Kordestani, A. Shokrollahi, R. Aghaei and A. J. Blake, *Inorg. Chim. Acta*, 2011, **370**, 141.

37 H. Aghabozorg, F. Ramezanipour, J. Soleimannejad, M. A. Sharif, A. Shokrollahi, M. Shamsipur, A. Moghimi, J. A. Gharamaleki, V. Lippolis and A. J. Blake, *Pol. J. Chem*, 2008, **82**, 487.

38 Z. Aghajani, H. Aghabozorg, E. Sadr-Khanlou, A. Shokrollahi, S. Derki and M. Shamsipur, *J. Iran. Chem. Soc.*, 2009, **6**, 373.

39 A. Shokrollahi, M. Ghaedi, H. R. Rajabi and M. S. Niband, *Spectrochim. Acta*, 2008, **71A**, 655.

40 A. E. Martell and R. J. Motekaitis, *Determination and Use of Stability Constants*, VCH, New York, 2nd edn, 1992.

41 (*a*) T. J. Mooibroek, P. Gamez and J. Reedijk, *CrystEngComm*, 2008, **10**, 1501; (*b*) M. Egli and S. Sarkhel, *Acc. Chem. Res.*, 2007, **40**, 197.

42 K. S. Seth, I. Saha, C. Estarellas, A. Frontera, T. Kar and S. Mukhopadhyay, *Cryst. Growth Des.*, 2011, **11**, 3250.

43 R. Aydin and U. Özer, *Turk. J. Chem.*, 2006, **30**, 145.

44 M. M. E. Darj and R. Malinowski, *Anal. Chem.*, 1996, **68**, 1593.

45 S. A. Bychkova, A. V. Katrovtseva and E. V. Kozlovskii, *Russ. J. Coord. Chem.*, 2008, **34**, 93.

46 A. Albert, R. Goldacre and J. Philips, *J. Chem. Soc.*, 1948, 2240.

47 H. Aghabozorg, F. Manteghi, M. Ghadermazi, M. Mirzaei, A. R. Salimi, A. Shokrollahi, S. Derki and H. Eshtiagh-Hosseini, *J. Mol. Struct.*, 2009, **919**, 381.

48 J. B. English, A. E. Martell, R. J. Motekaitis and I. Murase, *Inorg. Chim. Acta*, 1997, **258**, 183.

49 L. H. J. Lajunen, R. Portanova, J. Piispanen and M. Tolazz, *Pure Appl. Chem.*, 1997, **69**, 329.

50 M. Taha and M. M. Khalil, *J. Chem. Eng. Data*, 2005, **50**, 157.

